Defining the importance of the arginine loop region of protegrin-1 for antimicrobial activity towards colistin-resistant *Klebsiella pneumoniae*.

Christina DeBarro[a], Sofia Assent[a], Hannah Makhecha[a], Noor Radde[ghij], Rakesh Krishnan[bcde], Justin Randalf, Cesar de la Fuente-Nunez[bcde], and Renee M. Fleeman[a]*

[a] Division of Immunity and Pathogenesis, Burnett School of Biomedical Sciences, College of Medicine, University of Central Florida. Orlando, FL 32837

[b] Machine Biology Group, Departments of Psychiatry and Microbiology, Institute for Biomedical Informatics, Institute for Translational Medicine and Therapeutics, Perelman School of Medicine, University of Pennsylvania. Philadelphia, PA 19104, USA.

[c] Departments of Bioengineering and Chemical and Biomolecular Engineering, School of Engineering and Applied Science, University of Pennsylvania. Philadelphia, PA 19104, USA.

[d] Penn Institute for Computational Science, University of Pennsylvania. Philadelphia, PA 19104, USA.

[e] Department of Chemistry, School of Arts and Sciences, University of Pennsylvania, Philadelphia, Pennsylvania, USA.

[f] Department of Biological and Biomedical Systems, University of Missouri-Kansas City. Kansas City, MO 64110, USA.

[g] Harvard University, Ragon Institute MGH, Cambridge, MA 02139, USA

[h] Massachusetts Institute of Technology, Cambridge, MA, 02139, USA

[i] Harvard University, Boston, MA, 02115, USA

[j] Harvard University, Harvard Medical School, Boston, MA, 02115, USA

*Correspondence: Renee.Fleeman@ucf.edu

26 ORCID account = https://orcid.org/0000-0001-7103-461X

27

28 **Keywords**: *Klebsiella pneumoniae*, antimicrobial peptide, bacterial resistance, genetic screening

29 **Summary**

30 *Carbapenem resistant Klebsiella pneumoniae* extreme drug resistance has warranted the use of colistin
31 as a last-resort antibiotic but these isolates are now displaying increasing rates of colistin resistance.
32 This is in large part due to the modifications made to the lipid A by the PhoPQ two component system.
33 Host defense peptides (HDPs) are like colistin in that they are both positively charged and display
34 amphipathic character, however are not impacted by lipid A modifications to the extent of colistin. To
35 understand how HDPs can penetrate colistin resistant membranes we performed a deep mutational
36 scanning analysis of protegrin-1 and revealed that amino acids mutations that resulted in alteration of
37 peptide structure had more impact on antimicrobial activity than a reduction in charge. Probing single
38 and double amino acid variants using membrane analysis and molecular modeling revealed the loss of
39 antimicrobial activity correlated with decreased inner membrane leakage and pore modeling predicting
40 decreased pore size.

41

42 **Introduction**

43 Multidrug-resistant *Klebsiella pneumoniae* is responsible for a wide array of healthcare-associated
44 infections throughout the globe [1-8]. More specifically, as of 2024, the World Health organization has
45 declared carbapenem-resistant *K. pneumoniae* the top priority pathogen [9]. Colistin, a last resort
46 antibiotic, has been used in place of carbapenems to treat carbapenem-resistant *K. pneumoniae* [2, 3,
47 7, 10-12]. The two *K. pneumoniae* clonal groups most associated with global carbapenem resistance
48 are CG258 and CG15 [3, 13, 14]. While CG15 is more commonly associated with resistance to third-
49 generation cephalosporins, as of 2017 CG258 was responsible for approximately 70% of carbapenem-
50 resistant infections, with cases documented globally [3, 8]. Within this clonal group consists of three
51 sequence types, ST258, ST512, and ST11. Of these sequence types, ST258 has been associated with
52 the majority of carbapenem resistant outbreaks as well as global dissemination of carbapenemases [8,
53 13, 15, 16]. Importantly, we are now finding an increase in colistin resistance with ST258 clinical
54 isolates [7, 17-20].

55

56 Polymyxin B and E (colistin) are cationic cyclic lipopeptides with a charge of +5 that bind to the
57 lipopolysaccharides on the outer membrane of Gram-negative bacteria [10, 21-24]. More specifically,
58 the positively charged diaminobutyric acid residues of colistin bind to the negatively charged phosphate
59 groups on the lipid A portion of a lipopolysaccharide molecule (LPS), displacing the divalent cations
60 already present. This allows the hydrophobic tail of colistin to penetrate the outer membrane, resulting
61 in local membrane curvature. Eventually, colistin will form aggregates within the outer membrane,
62 resulting in structural instabilities. These instabilities allow colistin to cross the lipid bilayer and access
63 the inner membrane. At the inner membrane colistin will cause membrane thinning that will result in
64 cytosolic leakage and bacterial cell death [10, 21-24]. Colistin resistance in *K. pneumoniae* has been
65 largely attributed to the modifications on the outer membrane that alter the charge or structure of the
66 lipid A portion its lipopolysaccharides (LPS) [10, 21-24]. The overall charge of the bacterial membrane
67 can be increased by the replacement of negatively charged phosphates on the lipid A molecule by

68 positively charged chemical groups such as phosphoethanolamine (PEtN) and 4-amino-4-deoxy-L-
69 arabinose (L-Ara4N) [10, 21-24]. This will reduce colistin's affinity for the bacterial cell due to the
70 disruption of the initial electrostatic interaction. Furthermore, the acyl chains of a lipid a molecule can be
71 altered to increase the rigidity of the bacterial membrane, resulting in the mechanistic expulsion of
72 colistin and thereby resistance [22, 25]. The PhoPQ two-component system has been shown to be a
73 global regulator implicated in colistin resistance in Gram-negative bacteria, including *K. pneumoniae*
74 [26-29]
75
76 Host defense peptides are not equally affected by the modifications to the LPS that cause resistance to
77 polymyxins [30-32]. Compared to colistin that directly targets lipid A to displace the stabilizing cations
78 [10, 21-24], host defense peptides interact more generally with the LPS having multiple mechanisms of
79 membrane disruption. These include the 'detergent like' carpet model or the formation of pores through
80 the torodial pore and barrel-stave models [33-36]. Previous work describing host defense peptide
81 antimicrobial activity towards *K. pneumoniae* revealed that peptides with increased backbone steric
82 hinderance had improved activity, in particular towards colistin-resistant ST-258 *K. pneumoniae* strain
83 MKP103 [37, 38]. This suggests that not all host defense peptides are affected equally by the
84 modifications providing colistin resistance and there are important physiochemical properties that allow
85 them to retain antimicrobial activity towards colistin-resistant Gram-negative pathogens.
86
87 Here we describe the investigation into the strong antimicrobial activity of protegrin-1 towards colistin-
88 resistant *K. pneumoniae* MKP103 through a multi-level analysis (**Figure 1**). Deep mutational peptide
89 scanning revealed specific positions necessary for antimicrobial activity in protegrin-1. Furthermore, we
90 found intricate changes to secondary structure could impact antimicrobial activity, while comparatively
91 larger changes to the positive charge of the peptide were needed to impact activity. Specifically, within
92 the triple arginine motif of protegrin-1 a proline mutation decreases antimicrobial activity at position 9
93 but not at position 11. Mutation of a second arginine residue within this region, regardless of the

position of the proline resulted in complete loss of antimicrobial activity. Investigation into the peptide variants membrane interactions demonstrated changes in cytosolic leakage, which corresponded to the respective activity of our proline peptide variants. Moreover, despite a loss of activity we found an increase in outer membrane disruption with our inactive double mutation peptide variants. Molecular modeling revealed a distinct reduction in diameter and overall pore collapse of the modeled beta-sheet variant octameric pores as well as the rapid loss of beta-sheet character in the variants' monomeric models. These findings challenge the currently set precedent of colistin resistance being largely attributed to differences in charge, where we see with protegrin-1 even with the cysteine bonds in place, intricate changes in structure can impact pore formation in colistin-resistant *K. pneumoniae*.

105 **Results**

106 **Host defense peptides do not equally bypass *K. pneumoniae* MKP103 PhoP acquired polymyxin**

107 **resistance**

108 An increasing number of *K. pneumoniae* isolates are becoming resistant to the last resort antibiotic
109 colistin [7, 17-20]. Colistin is positively charged and displays amphipathic structure, characteristics
110 shared by host defense peptides [21, 39-41]. Host defense peptides are a stressor that is responded to
111 by the PhoPQ two-component system, although the modifications to the LPS causing colistin resistance
112 does not equally apply to all host defense peptides [30-32, 42]. To expand on our understanding of the
113 varying impact of PhoPQ mediated colistin resistance on different host defense peptides first we
114 validated *K. pneumoniae* MKP103 resistance to polymyxins was mediated by upregulation *phoP* and
115 tested the impact of this resistance to antimicrobial activity of different classes of host defense peptides.

116

117 To validate PhoPQ mediated polymyxin resistance in *K. pneumoniae* MKP103, we first identified the
118 minimal inhibitory concentration (MIC) of polymyxin B and colistin (polymyxin E) next to other well
119 published *K. pneumoniae* strains. We found minimal polymyxin resistance with hypervirulent *K.*
120 *pneumoniae* NTUH [43] and KPPR1S [44], drug-resistant *K. pneumoniae* ATCC 700603 [45], and type
121 strain *K. pneumoniae* ATCC 13883 [46] (MICs < 1 μmol L^{-1}) when compared to *K. pneumoniae*
122 MKP103, a genetically modified ST-258 strain used for the creation of a transposon library (MIC 27
123 μmol L^{-1}) [47, 48] (**Table S1, Figure 2A**). We then determined the baseline expression levels of
124 response regulator *phoP* with RT-qPCR to compare to their respective polymyxin resistance [49, 50]
125 and found high levels of *phoP* expression correlated with colistin resistance in *K. pneumoniae* MKP103
126 (**Figure 2A,Figure S1**). Therefore, we determined *K. pneumoniae* MKP103 to be the ideal screening
127 candidate for our investigation into PhoPQ mediated colistin resistance.

128

129 To determine a candidate host defense peptide for our deep mutational scanning, we used the parental
130 MKP103 and its *ΔphoP* transposon mutant (KPNIH1_10030-701::T30) and compared MICs of different

131 structural classes of antimicrobial peptides (**Table 1**). As shown with previous studies on colistin
132 resistance [30-32], we found that PhoP mediated polymyxin resistance does not extend equally to host
133 defense peptides compared to polymyxin B and E, which had a 256-fold change between the parental
134 strain and *ΔphoP* mutant (**Figure S1, Figure 2B**). Specifically, the largest fold change in MIC between
135 the parental strain and *ΔphoP* mutant was with indolicidin (16-fold), an extended host defense peptide
136 with a random coil structure (**Figure 2B**). Furthermore, when testing alpha-helical peptides, we saw LL-
137 37 and melittin (8-fold change MIC) were similarly affected by PhoP mediated resistance while cecropin
138 A was slightly less affected (4-fold change MIC). When testing beta-sheet peptides, protegrin-1 and
139 arenicin both had a 4-fold change in MIC between the parental strain and *ΔphoP* mutant. Finally, as
140 expected due to its internal mechanism of killing [51], the polyproline peptide bac7 (1-35) had only 2-
141 fold change in MIC between the MKP103 parental strain and *ΔphoP* mutant. For a comparison of the
142 peptide backbone steric hindrance of the tested host defense peptides following up on previously
143 observed finding [37], we created Ramachandran plots of the host defense peptides displaying the
144 dihedral rotation angles of each amino acid residue. The alpha helical host defense peptides (ll-37,
145 cecropin, and melittin) plotted within the right-handed alpha-helical region of the Ramachandran plot
146 (**Figure 2C**) revealing the precise angles needed to form a helical protein [52-54] due to the flexibility of
147 the peptide backbone. The beta-sheet peptides (protegrin-1 and arenicin) and extended peptides (bac7
148 (1-35) and indolicidin) plotted within the beta-sheet/collagen triple helix region of the Ramachandran
149 plot (**Figure 2D, and 2E**), a region known for being the most restrictive for amide bond rotation [54].
150 Although indolicidin localized within this region, the individual amino acids displayed a range of
151 flexibility, shown by the spread on the Ramachandran plot. Collectively, host defense peptides that had
152 tight localization to the beta-sheet/collagen triple helix region of the Ramachandran plot were less
153 impacted by *K. pneumoniae* MKP103 PhoP mediated colistin resistance. Protegrin-1, along with having
154 a low fold change between parental MKP103 and *ΔphoP* mutant, also has a well characterized
155 structure and mechanism of action [55-57]. Furthermore, this peptide's two disulfide bonds, which are

156 responsible for protegrin-1's tightly constraint structure, are ideal for molecular dynamic simulations
157 [58]. For these reasons we chose this peptide as our candidate for deep mutational scanning to
158 investigate the ability of this host-defense peptides to bypass *K. pneumoniae* colistin resistance.
159

160 **Protegrin-1 deep mutational scanning library shows reveals charge and structure are important**
161 **for antimicrobial activity towards colistin-resistant *K. pneumoniae* MKP103**

162 To understand the importance of individual amino acids to the antimicrobial activity of beta-sheet
163 peptide towards colistin-resistant *K. pneumoniae* we next aimed to perform deep mutational scanning
164 analysis of the beta-sheet peptide protegrin-1. For this we utilized the Surface Localized Antimicrobial
165 Display (SLAY) system that was designed to display antimicrobial peptides on the surface of Gram-
166 negative bacteria to capitalize on the high-throughput advantages of next-generation sequencing [59].
167 Further optimization of this platform led to the development of deep mutational scanning with SLAY
168 (dmSLAY), using this tool to assess protegrin-1 and describe features driving membrane selectivity
169 between bacteria and mammalian cells [60]. As previously described, the creation of the protegrin-1
170 dmSLAY ensured a high level of conservation was given to the mixed base primer sequence (**Table**
171 **S2, Figure S2**), with the possibility of 7-12 changes at each amino acid residue, resulting in 1-9
172 mutations per peptide variant. We aimed to expand on this impactful study by testing the protegrin-1
173 dmSLAY library in colistin-resistant *K. pneumoniae* MKP103.

174

175 We collected the plasmid-based library from colistin-resistant *K. pneumoniae* MKP103 following growth
176 for four hours with and without plasmid induction with isopropyl β-D-thiogalactoside (IPTG). To predict
177 antimicrobial activity of the peptide variants in our library, we used next generation sequencing to
178 quantify the plasmids from the induced versus the uninduced population **(Table S3)**. Sequences that
179 express for an active peptide variant are removed from the population of plasmids following induction

180 resulting in a negative log2 fold change in reads. With the goal to understand what amino acids were
181 implicated in retaining the antimicrobial activity of protegrin-1, we looked for retention within the
182 population of peptide variants rather than removal and used a log2 fold change value of 0 or higher is
183 indicative of lack of antimicrobial activity. Overall, we identified approximately 1700 peptide sequence
184 variants lacking activity against *K. pneumoniae* MKP103 **(Figure 3A; Supplemental data file 1).** To
185 determine which specific amino acid residues were necessary to bypass colistin resistance, we chose
186 to investigate individual mutations that occurred most often in our inactive peptide variant population,
187 rather than testing peptide variants from the screen **(Table S4)**. We had some individual amino acid
188 mutations that occurred only ≤20 peptide variants. However, we were intrigued to find several amino
189 acid mutations that were in the majority of peptide variants retained in the population **(Table 2, Figure**
190 **3B).** We chose not to investigate mutations with less than 25 occurrences, those that did not involve an
191 amino acid class change, and those that impacted disulfide bonds, as literature has already shown their
192 importance for protegrin-1's antimicrobial activity [61, 62]. This resulted in the selection of five individual
193 mutations in different structural regions of protegrin-1 to investigate their effects alone on the surface
194 display system (**Figure 3B**). Specifically, the glycine at position to mutated to an arginine (G2R)
195 increasing the charge of the unstructured tail region was found 316 times within the population of
196 peptide variants that had a log2 fold change >0. A leucine mutation to an isoleucine (L5I) and
197 phenylalanine to leucine (F12L) within the beta-sheet region were found in 218 and 834 of peptide
198 variants retained in the population, respectively. Finally, we found mutations in 2 arginine residues of
199 the triple arginine loop region (R9P and R10L) times 295 and 299 within the population of peptide
200 variants retained in the population, respectively and these variants most often occurred together.

201

202 To test the selected individual mutations using the SLAY platform, we cloned the single amino acid
203 variants of protegrin-1 into the genetic screening system **(Table S5, S6)** and induced the plasmid in
204 colistin-resistant *K. pneumoniae* MKP103 over a four-hour period enumerating CFU mL^{-1}. When testing

205 the parental peptide displayed on the surface with 1 mM IPTG induction we found there was a 5-log
206 reduction in CFU mL^{-1} when compared to an uninduced plasmid control, and bacteria harboring the
207 system with a tandem influenza hemagglutinin peptide (2xHA) as a negative control **(Figure 3C)**.
208 Testing the individual amino acid mutations next to the parental peptide, we found the mutation of an
209 arginine to leucine (R10L), glycine to arginine (G2R), leucine to isoleucine (L5I), and phenylalanine to
210 leucine (F12L) mutations displayed minimal change in CFU mL^{-1} compared to the surface display of the
211 parental peptide (**Figure 3D).** However, when introducing a proline mutation at position 9 (R9P), we
212 saw this single mutation could reduce the activity of the peptide towards colistin-resistant *K.*
213 *pneumoniae* MKP103 by 2-fold compared to our parental peptide**.** Intriguingly, we found the arginine to
214 proline mutation in our next-generation sequencing occurred approximately 89% of the time with an
215 arginine to leucine mutation at position 10 (R9P, R10L). Therefore, we also tested these amino acid
216 mutations together using SLAY and found the complete loss of activity of the peptide with two arginine
217 amino acid residues mutated within the triple arginine motif (**Figure 3D**). Overall, our deep mutational
218 scanning of protegrin-1 identified candidate amino acids that are important for antimicrobial activity
219 towards colistin-resistant *K. pneumoniae.* Although many of these mutations needed additional
220 mutations for a reduction in antimicrobial potential, we identified a single arginine to proline mutation at
221 position 9 within the beta-sheet to turn transition region of the triple arginine motif that alone could
222 impact antimicrobial activity and the complete loss of activity when this was accompanied by a second
223 mutation within this region.

224

225 **The arginine to proline mutation impedes antimicrobial activity only in the beta-sheet to turn**
226 **transition region of the protegrin-1 arginine loop**

227 With the intriguing findings from our deep mutational scanning of protegrin-1 arginine loop beta-sheet to
228 turn transition region, we had the single (R9P and R10L) and double (R9P, R10L) protegrin-1 variants

229 synthesized to test their antimicrobial activity towards of *K. pneumoniae* MKP103 parental strain next to
230 the *ΔphoP* mutant, mutants downstream of PhoP regulon, and a panel *K. pneumoniae* clinical isolates.
231 In addition to testing amino acids discovered in our dmSLAY analysis, we also synthesized a single and
232 double variant with a proline mutation at position 11 (R11P and R10L, R11P). This placed the proline
233 amino acid substitution within the peptide's turn region rather than its beta-sheet to turn transition
234 region **(Table 3)** and test the importance of the changes to peptide positive charge versus the
235 secondary structure that were introduced by the R9P mutation. Furthermore, in order to investigate the
236 position itself rather than the amino acid mutation found in that position, we also synthesized alanine
237 and lysine single peptide variants at positions 9 (R9A and R9K) and 11 (R11A and R11K).

238 When testing antimicrobial activity towards the colistin-resistant *K. pneumoniae* MKP103 used for
239 screening, both the R9P and R10L variant displayed a reduction of activity compared to protegrin-1
240 (MIC 15.23 and 15.11 μmol L^{-1}, respectively) **(Table 4)**. We observed that despite a reduction in charge
241 (charge +5), the R11P variant retained the same level of antimicrobial activity toward our colistin-
242 resistant isolate as protegrin-1 (charge +6) (MICs 3.8 μmol L^{-1} respectively). When testing the double
243 mutant variants (R9P, R10L and R10L, R11P) (charge +4), we found they both lost activity towards *K.*
244 *pneumoniae* MKP103 (MIC >30 μmol L^{-1}). Interestingly, when substituting either position 9 or 11 with an
245 alanine (R9A or R11A) we found the similar antimicrobial activity to the R9P peptide variant (MICs
246 15.41,15.41, 15.23 μmol L^{-1}, respectively). However, when substituting position 9 and 11 with a lysine
247 (R9K or R11K) we have smaller changes in activity, indicating charge retention at these positions has
248 variable impacts on antimicrobial activity (MICs 3.75 and 7.50 μmol L^{-1}, respectively).

249

250 To broaden the impact of our findings beyond *K. pneumoniae* MKP103 we selected colistin-resistant
251 clinical isolates from the Mult-drug-Resistant Organism Repository and Surveillance Network (MRSN)
252 *K. pneumoniae* diversity panel to test the peptide variants against [63]. We found although the majority

253 of isolates (64 MRSN isolates) were colistin sensitive (MIC ≤ 0.87 μmol L^{-1}), there were 31 isolates that
254 displayed moderate colistin resistance (MIC 1.73-6.92 μmol L^{-1}), and 5 isolates (MRSN 13768, 430414,
255 430405, 560539, and 728987) that displayed elevated colistin resistance (MICs >13 μmol L^{-1}) **(Table**
256 **S7)**. Of note, two isolates, MRSN 13768 and 430414, had colistin MICs comparable to that of *K.*
257 *pneumoniae* MKP103 (27.69 μmol L^{-1}). However, when assessing our protegrin-1 peptide variants
258 towards these clinical isolates, we found that majority our MICs were relatively similar to the parental
259 peptide protegrin-1, with the R9P single variant displaying the least antimicrobial activity (3.81 μmol L^{-1})
260 (**Figure 4A**). When testing the double mutant variants (R9P, R10L and R10L, R11P) we found they lost
261 antimicrobial activity towards 3 of the 5 colistin resistant MRSN clinical isolates. Specifically, MRSN
262 430405 (colistin MIC 27.69 μmol L^{-1}), was completely resistant to the beta turn double mutant peptide
263 variant (R10P, R11L MIC 31.09 μmol L^{-1}) but not the beta sheet double variant (R9P, R10L MIC 7.77
264 μmol L^{-1}). Furthermore, MRSN 560539 (colistin MIC 13.85 μmol L^{-1}) displayed the same level of
265 resistance to both beta sheet and beta turn double variants (MICs 15.54 and 15.55 μmol L^{-1},
266 respectively) and MRSN 728987 (colistin MIC 13.85 μmol L^{-1}) was slightly more sensitive to the double
267 mutant peptide variants (MIC 7.77 μmol L^{-1}).

268

269 When assessing the changes in MIC in the absence of PhoP regulon induction using the *ΔphoP*
270 mutant, we found the beta sheet peptide variants (R9P and R9P, R10L) had a larger fold-change in
271 antimicrobial activity between the mutant and parental *K. pneumoniae* MKP103 than the beta turn
272 variants (R11P and R10L, R11P) **(Figure 4B)**. Of note, when comparing this the parental peptide
273 protegrin-1, we found the beta sheet peptide variants (R9P and R9P,R10L) displayed the same 32-fold
274 decrease in MIC toward the *ΔphoP* mutant as protegrin-1, whereas the beta turn peptide variants
275 (R10L, R11P, and R10L, R11P) only displayed an 8-, 4-, and 8-fold decrease in MIC towards the
276 *ΔphoP* mutant, respectively. Furthermore, we tested *K. pneumoniae* MKP103 transposon mutants of

277 downstream genes within the PhoP regulon, involved in modifying either the rigidity or charge of the
278 LPS [25, 42]. Specifically, PagP transfers a palmitate group to a lipid A molecule and PagL removes an
279 acyl group, altering the membrane's fluidity and permeability [25, 64], while ArnT and PmrB are
280 involved in the addition of a 4-amino-4-deoxy-L-arabinose (L-Ara4N) on lipid A, increasing the positive
281 charge of the outer membrane [25]. We found no difference between the MICs of parental protegrin-1,
282 the beta sheet peptide variants (R9P and R9P, R10L), indicating a combination of LPS modifications
283 are necessary for the sensitivity displayed by the *ΔphoP* mutant (**Figure 4B**). Interestingly, although the
284 beta turn peptide variants did not show as much of a fold-change in MICs with the *ΔphoP* mutant as the
285 beta sheet peptide variants and parental peptide protegrin-1, we found a slight fold-change increase in
286 MIC between the downstream PhoP regulon mutants compared to the parental *K. pneumoniae*
287 MKP103. Specifically, when testing the R11P variant, the *ΔpagL and ΔpagP* transposon mutants
288 (KPNIH1_07455-208::T30 and KPNIH1_13050-101::T30, respectively) displayed 4-fold decrease in
289 MIC (MIC 0.96 μmol L^{-1}) **(Table S5)** compared to *K. pneumoniae* MKP103 (MIC 3.81 μmol L^{-1}), while
290 the *ΔarnT and ΔpmrB* transposon mutants (KPNIH1_24880-114::T30 and KPNIH1_08200-303::T30)
291 displayed 2-fold decrease in MIC (MICs 1.90 μmol L^{-1}). Finally, the beta turn double mutant peptide
292 variant (R10L, R11P) all four PhoP regulon transposon mutants displayed a 2-fold increase in MIC.

293

294 Upon investigation of positions 9 (beta sheet) and 11 (beta turn) within protegrin-1 with alanine and
295 lysine amino acid substitutions, we find much more variability within our colistin resistant clinical
296 isolates than the mutations that came from the dmSLAY analysis of *K. pneumoniae* MKP103 **(Figure**
297 **4C)**. Specifically, alanine substitution at position 9 (beta turn) had MICs of 15.42 and 30.84 μmol L^{-1}
298 towards MRSN 13768 (colistin MIC 27.79 μmol L^{-1}) and MRSN 430505 (colistin MIC 13.85 μmol L^{-1}),
299 respectively. MRSN 430505 also displayed higher resistance towards the peptide variant with alanine
300 substituted in the turn region (R11A MIC 15.00 μmol L^{-1}) and lysine substituted in the sheet region (R9K

301 MIC 15.42 μmol L^{-1}). These peptides also displayed less variability between the antimicrobial activity
302 towards the parental strain *K. pneumoniae* MKP103 and the PhoPQ regulon transposon mutants.
303 Contrary to our variants identified from the initial screening, we found increased fold change in activity
304 between the parental strain and PhoP regulon transposon mutants **(Figure 4D)**. Interestingly, we see
305 these less bulky substitutions at position 11 variants (R11A, R11K) were more impacted by the
306 downstream individual PhoP regulated changes than the position 9 variants (R9A, R9K). Specifically,
307 R11A peptide variant when tested against the *ΔpagP, ΔpagL, and ΔarnT* transposon mutants resulted
308 in a 16-fold decrease in MIC compared the parental strain, and *ΔpmrB* transposon mutant had an 8-fold
309 lower MIC. When testing our peptide variants against other Gram-Negative bacteria we find that
310 regardless of variant, *Burkholderia thailandensis* [65] exhibits complete resistance, while *Acinetobacter*
311 *baumannii* [66] and both *Escherichia coli* [60, 67, 68] strains display high sensitivity to all peptide
312 variants, suggesting these peptide variants identified in this study are unable to bypass Gram-negative
313 bacteria with high levels of colistin resistance **(Table S8)**. Collectively, we found when proline was
314 introduced to the turn region (R11P) of the triple arginine motif had less impact on the antimicrobial
315 activity than when placed in the beta-sheet to turn transition region (R9P) and that removing an
316 additional arginine from the triple arginine motif regardless of the proline position completely abolished
317 antimicrobial activity towards colistin-resistant *K. pneumoniae* MKP103.

318

319 **Protegrin-1 double mutant variants with reduced charge display greater disruption of colistin-**
320 **resistant outer membrane**

321 We found modifications to the outer membrane LPS by the PhoP regulon increase resistance to our
322 beta sheet peptide variants more than our beta turn variants, indicating a role in that amino acid in
323 bypassing colistin resistance LPS modifications. Furthermore, we found a dichotomy between colistin
324 resistance and peptide variant resistance when testing the MRSN clinical isolates, where the
325 moderately elevated colistin resistant clinical isolates (MIC 1.73-6.92 μmol L^{-1}), are more resistant to

326 the double mutant peptide variants compared to the more colistin resistant clinical isolates (MIC 13
327 μmol L^{-1}). Therefore, when assessing the mechanism of action of the peptide variants compared to the
328 protegrin-1 parental peptide, we wanted to first probe the outer membrane integrity following treatment
329 as protegrin-1 must interact and bypass the outer membrane before forming a pore at the inner
330 membrane. To evaluate changes in outer membrane permeability, we used N-Phenyl-1-naphthylamine
331 (NPN), a hydrophobic small molecule impermeable to an intact outer membrane that fluoresces weakly
332 with increased fluorescence observed upon outer membrane disruption [69-71].
333
334 When testing the parental strain *K. pneumoniae* MKP103, our single point mutations (R9P, R10L and
335 R11P) at 31 μmol L^{-1} behave similarly to protegrin-1 but also polymyxin B (MIC 27 μmol L^{-1}) **(Figure**
336 **5A).** Unexpectedly, the double mutation variants (R9P, R10L and R10L, R11P) when tested at 31 μmol
337 L^{-1} display higher fluorescence of NPN than parent protegrin-1, indicating increased disruption of the
338 outer membrane of colistin-resistant *K. pneumoniae* MKP103 **(Figure 5B).** Interestingly, when testing
339 our *ΔphoP* mutant **(Figure 5C and 5D)** and downstream mutants modifying both charge and fluidity, all
340 peptide variants display higher fluorescence of NPN (**Figure S3)**. Our beta sheet double peptide variant
341 in these cases had activity similar to or less than our parent peptide. Comparing the endpoint
342 fluorescence across isolates we find the least amount of disruption from our single mutant peptide
343 variants with our *ΔpagL* transposon mutant **(Figure 5E)**. We also find that in every isolate our more
344 active variant (R11P) is less effective at disrupting the outer membrane compared to our less active
345 variant (R9P). When observing endpoint fluorescence of our double mutant variants we also see the
346 least amount of disruption with our *ΔpagL* transposon mutant **(Figure 5F)**. When testing our most
347 colistin resistant clinical isolates, the peptide variants also display higher fluorescence of NPN **(Figure**
348 **S4)**. However, our beta turn double peptide variant (R10L, R11P) disrupts the outer membrane more
349 effectively than the beta sheet double peptide variant (R9P, R10L) **(Figure S4)**. Overall, we account for

350 some but not all of the changes in antimicrobial activity towards parental MKP103 with differences in
351 peptide interactions within the outer membrane.

352

353 **The arginine to proline mutation in the beta-sheet transition limits cytosolic leakage in single**
354 **and double mutation variants**

355 Protegrin-1 has a membrane disruptive mechanism of action and has been described to form pores in
356 the inner membrane of the bacteria [55, 72]. To assess the peptide variants loss of membrane
357 disruptive killing, we investigated their ability to depolarize and cause leakage of the inner membrane of
358 colistin-resistant *K. pneumoniae* MKP103. Depolarization is caused by many host defense peptides
359 including those that do not form pores [73, 74]. However, predominantly pore forming peptides can
360 cause leakage of the cytoplasmic components [75, 76]. With the lesser degree of outer membrane
361 disruption observed with our more active peptide variants, we hypothesize they are penetrating to the
362 inner membrane but their mechanism of interaction with the inner membrane is variable depending on
363 the mutations introduced. We evaluated changes in membrane polarity across the inner membrane with
364 3,3'-dipropylthiadicarbocyanine Iodide ($DiSC_3$) [77]. This cationic dye inserts into polarized inner
365 membranes quenching its fluorescence and depolarization of the inner membrane results in release of
366 the dye and an increase in fluorescence. When testing the single mutation variants (R9P, R10L and
367 R11P) at 31 μmol L^{-1}, only our beta sheet single peptide variant (R9P) depolarized the inner membrane
368 of resistant *K. pneumoniae* MKP103 to the extent of the parent protegrin-1, while our more active beta
369 turn variant (R11P) depolarized the inner membrane less than our parent peptide **(Figure 6A)**. Our less
370 active beta turn variant (R10L) comparatively exhibited the least amount of depolarization toward
371 MKP103. When testing the double mutation peptide variants (R9P, R10L and R10L, 11P) at 31 μmol L^{-}
372 ^{1}, both variants depolarized the inner membrane less than the parent protegrin-1 **(Figure 6B)**. Overall,
373 all peptide variants depolarized the inner membrane greater than the polymyxin B, tested at 31 μmol L^{-}
374 ^{1}. We continued our investigation of changes in inner membrane polarity with our *ΔphoP* transposon

375 mutant. We found that unlike our parental isolate, both our R9P and R11P depolarize the inner
376 membrane to the same extent as parent protegrin-1 **(Figure 6C)**. Our beta turn single variant (R10L)
377 does continue to have the lowest depolarization ability of all our peptide variants. This trend continues
378 with our double variants, where both our beta turn and beta sheet double variants exhibit depolarization
379 on par with our parent peptide **(Figure 6D)** rather than lower depolarization, as seen in our parent
380 MKP103.
381
382 To assess for changes in cytoplasmic leakage, we utilized ortho-nitrophenyl-β-galactoside (ONPG), a
383 substrate that is hydrolyzed to ortho-nitrophenol (ONP) by cytoplasmic β-galactosidase [78]. When
384 testing the single mutation peptide variants (R9P and R11P) at 31 μmol L^{-1} , we found although both
385 variants resulted in leakage similar to the parental protegrin-1, there was a delay in the time to cause
386 equal leakage (**Figure 7A**). Specifically, the R11P peptide variant matched the ONP levels induced by
387 the parental protegrin-1 after 25 minutes, while the R9P peptide variant did not match the leakage until
388 40 minutes. Surprisingly, our beta turn single variant (R10L) resulted in very little inner membrane
389 leakage, displaying levels less than our inactive polymyxin B. When testing the double mutation
390 variants (R9P, R10L and R10L, R11P) at 31 μmol L^{-1}, our beta sheet double peptide variant resulted in
391 a decrease in the ONP levels compared to the parental protegrin-1 and displayed levels similar to the
392 inactive polymyxin B (**Figure 7B**). The beta turn double peptide variant displayed a delay in
393 fluorescence compared to the parental protegrin-1 at this concentration **(Figure 7B)**. Investigation with
394 our *ΔphoP* transposon mutant resulted in an overall inability to effectively disrupt the inner membrane
395 with all peptide variants **(Figure 7C and D)**. We also find that all peptide variants behave similarly to
396 parent protegrin-1 regardless of differences in antimicrobial activity. Our beta turn single variant (R10L),
397 however, still behaves similarly to our inactive polymyxin B. **(Figure 7C)**. Collectively, our results show
398 that all peptide variants depolarize the inner membrane but changes in cytoplasmic leakage correlate
399 best with the peptide variants MICs.
400

401 **Molecular modeling shows octameric pore collapse and loss of beta sheet character in beta**
402 **sheet peptide variants.**

403 We found the membrane leakage to correspond to the decrease in antimicrobial activity observed with
404 our peptide variants suggesting a deficiency in the pore formation potential of the peptide variants.
405 Alpha helical peptides like ll-37 have been shown to dimerize before insertion into the membrane [79].
406 However, protegrin-1 has been shown to dimerize within the phospholipid bilayer of the inner
407 membrane ultimately leading to octameric pore formation [55]. Therefore, to provide a full spectrum of
408 the potential of the mutations in the peptide variants we modeled the peptide variants before and after
409 interaction with the bacterial membrane, as well as their octameric pore conformations when fully
410 inserted. We also chose to eliminate our beta turn single peptide variant (R10L) due to its inability to
411 cause any inner membrane leakage.

412

413 We modeled our octameric pores utilizing AlphaFold2 with the sequences aligned in the N- to C-termini
414 direction. Images were visualized and diameter distances generated utilizing ChimeraX. Compared to
415 our parent peptide **(Figure 8A)**, our less active single peptide variant (R9P) **(Figure 8B)** exhibits a
416 reduction in diameter in our octameric pore model (~20Å to 11Å, respectively). In contrast, our more
417 active single peptide variant (R11P) **(Figure 8C)** changes the orientation of the hypothetical pore but
418 maintains pore diameter at ~20Å. When comparing our parent peptide to our double peptide variants
419 we find our beta sheet double peptide variant (R9P, R10L) also exhibiting a pore reduction **(Figure 8D)**
420 to ~14-15 Å, and our beta turn double peptide variant (R10L, R11P) **(Figure 8E)** maintained the pore
421 diameter (~ 18Å). This suggests that perhaps the monomeric structures involved in pore formation are
422 differentially impacted by our introduced mutations.

423

424 To better understand the peptide variants behavior within the octameric pore, we modeled our peptide
425 as monomeric subunits and observed how the structure of the peptide became altered in solution. To
426 do this we utilized GROMACS, a molecular dynamics software that uses different algorithms to model
427 the behavior of the peptide and its interactions with individual molecules over a span of time. These
428 mutations were modeled in an environment of 0.15M NaCl at 310K over the course of 100ns to observe
429 changes in the structural conformation of each peptide mutant [80]. We use Secondary Structure
430 Predictors (DSSP) to observe changes in beta-sheet character over the simulation period. Compared to
431 the parent peptide **(Figure 8F)**, the proline mutation at position 9 resulted in a shortened beta-sheet in
432 its initial structure and an early loss of beta sheet character, at approximately 4000 frames (40 ns) that
433 was never regained throughout the simulation **(Figure 8G)**. However, at position 11, the initial structure
434 remained close to that of the parent peptide and the loss of beta character occurred after the halfway
435 point of the simulation, at approximately 60000 frames (60 ns) (**Figure 8H).** When assessing the double
436 peptide variants, the beta sheet region variant (R9P, R10L) does display a minor level of beta-sheet
437 character throughout the simulation, however it is interwoven with regions of disorder. Furthermore, its
438 initial structure does have shorter beta sheets when compared to the parent peptide **(Figure 8F and**
439 **8I).** Finally, our beta turn double peptide variant, (R10L, R11P) results in no changes to its initial
440 structure when compared to the parent peptide. This double mutation fully loses its beta sheet
441 character at approximately 60000 frames (60 ns) and regains it at approximately 80000 frames (80 ns),
442 which may account for its ability to form a correctly oriented pore **(Figure 8E and 8J)**.
443
444 Protegrin-1 dimerizes before aggregating into an octameric pore inside the inner membrane. To better
445 assess how our mutations altered peptide structure we assessed changes in its ability to form a dimer.
446 Once again, we utilized GROMACs and an environment of both 0.15M NaCl at 310K and a general
447 Gram-Negative inner membrane, over the course of 100ns [80, 81]. Before and after snapshots were
448 taken to observe changes in the secondary structure of each mutated dimer compared to the parent
449 **(Figure 8K)**. Parent protegrin-1 does not seem to align itself as a dimer in the salt box at the beginning

or end of the simulation. This is also true in the Gram-Negative inner membrane simulation where it overlaps at the beta turn region at the beginning and orients across from itself after 100ns. This is unlike both single peptide variants **(Figure 8L and 8M)**. Both align themselves together at the beginning of the simulation. Our R9P only aligns one beta sheet at the end of the simulation, however, it does display a lengthened beta-sheet. This is unlike R11P, which does not display a lengthened beta sheet at the end of the simulation. Inside the Gram-Negative environment, both single mutant variants orient very similarly at the beginning of the simulation, however at the end they orient themselves diagonally in opposing directions. Our beta sheet double peptide variant found in the screen (R9P, R10L) also aligns with itself at the beginning of the simulation and displays some alignment towards the end **(Figure 8N)**. Our other beta turn double peptide variant, R10L, R11P also aligned itself at the beginning of the simulation **(Figure 8O)**. Unlike all the other mutations, however, there is no alignment at the end of the simulation. In the Gram-negative inner membrane model, both double peptide variants exhibit diagonal alignment of both of their beta sheets, albeit in opposing directions. Looking at how each dimer behaves over the course of the simulation, protegrin-1 has a larger and more variable center of mass than all our point mutations, suggesting a less stable conformation **(Figure S5A)**. Our mutated peptide variants all behaved similarly, having a lower center of mass compared to the parent peptide. This suggests less movement and could explain why there was partial alignment of the peptide variants in the salt environment after 100ns **(Figure 8K-O)**. Furthermore, there were fewer contacts that existed between the dimers of parent protegrin-1 over the course of the salt box simulation **(Figure S5B)**. Meaning this set of monomers were not interacting with each other, explaining why there is no alignment at the end of the simulation **(Figure 8K-O).** Aside from our RR910PL point mutations, all other mutations have a larger and about the same number of contacts across the simulations. Our RR910PL mutation had two instances of a higher number of contacts, from approximately 4000 to 6000 ns, and 8000 to 8500 ns. This change in the number of contacts may explain its change in alignment compared to our other point mutations. Within the context of our Gram-negative inner membrane simulation our parent peptide also exhibited a large center of mass compared to our peptide variants,

which could explain why at the end of the simulation they look as if on opposing sides of a potential pore **(Figure 8K, S5C)**. Furthermore, there is a decrease in the number of contacts between each chain over the course of the simulation **(Figure S5D)**. However, unlike in our salt box there is a much larger gap in the initial number of contacts. This could be due to how they initially intercalated within the inner membrane bilayer. Taken together these hypothetical models show our peptide variants with beta sheet (R9P and R9P, R10L) mutations impact pore formation and our monomeric subunits exhibit a rapid loss of beta sheet character not seen with our beta turn variants (R11P and R10L, R11P).

485 **Discussion**

486 Carbapenem *K. pneumoniae* resistant isolates are now acquiring resistance to the last resort antibiotic
487 known as polymyxin E or colistin [7, 17-20]. This resistance is attributed to modifications to the LPS by
488 the PhoPQ two component system [26-29]. Here we corroborate previous literature stating that host-
489 defense peptides are not equally affected by these LPS modifications as colistin [30-32,37,38],
490 especially protegrin-1 **(Figure 2B)**. The absence of resistance, combined with its well characterized
491 structure and robust antimicrobial activity [54-56] made protegrin-1 an ideal candidate to investigate
492 colistin resistance in *K. pneumoniae.*

493

494 Utilizing our dmSLAY genetic screening platform in combination with quantitative next generation
495 sequencing we found five amino acid mutations that were abundant in the population of plasmids
496 retained following 4-hour induction, indicating they may alter the antimicrobial activity of protegrin-1.
497 First, an arginine substituting a glycine (G2R) in the tail region, potentially altering charge localization of
498 the peptide to the point where it no longer retained activity. An isoleucine substituting a leucine (L5I) in
499 the first beta-sheet potentially adding more bulk to the peptide. A proline in the triple arginine motif
500 within the beta-sheet to turn transition (R9P) that could introduce a kink and potentially disrupting the
501 function of the peptide. Finally, a leucine in both the turn region (R10L) and second beta-sheet (F12L)
502 that would allow for less binding of the peptide when compared to an arginine or phenylalanine,
503 respectively. We also found that our beta sheet proline and beta turn leucine mutations (R9P, R10L)
504 most commonly occurred together in peptide variants retained within the population. To test the effects
505 of these mutations independently without other peptide modifications, we directly cloned them into our
506 surface display genetic platform and performed growth analysis, revealing the beta sheet region
507 arginine to proline (R9P) and beta turn region arginine to leucine (R10L) mutations has the greatest
508 impact on the antimicrobial activity of protegrin-1, and combining these mutations (R9P,R10L) resulted
509 in a complete loss of antimicrobial activity **(Figure 3D)**. Overall, we were surprised that more mutations
510 resulted in possible structural changes rather than changes to charge in the population retained in the

511 population in the dmSLAY analysis, because charge has been the major factor shown to contribute to
512 bypassing the Gram-negative membrane [82]. This included those that added arginine residues to the
513 unstructured tail region (G2R and G3R) increasing the charge of the peptide but not antimicrobial
514 activity.
515
516 We then synthesized peptide variants to validate the surface display system and test our hypothesis
517 that structure potentially supersedes charge. Specifically, we synthesized R11P and R10L, R11P
518 peptide variants that placed the proline residue in the turn region of the triple arginine motif rather than
519 the beta sheet transition region. We found then when testing these variants against MKP103 that our
520 R11P peptide variant retains antimicrobial activity and our R9P peptide variant loses activity, despite a
521 charge reduction on +1 in both peptide variants **(Table 4)**. Furthermore, when comparing the activity of
522 our peptide variants against MKP103 and transposon mutants of genes under the regulation of PhoP,
523 we find the fold change difference in activity is lower with our variants in the beta turn region versus the
524 beta sheet region **(Figure 4B)**. These modifications both resulted in a loss of charge but did not equally
525 lose antimicrobial activity, challenging the paradigm that charge is not necessarily most important
526 aspect in the ability of host defense peptide ability to overcome colistin resistance. To further test this
527 hypothesis, we tested the addition of alanine and lysine modifications to positions 9 and 11 on
528 protegrin-1. Surprisingly, we found these smaller amino acids when substituted at position 11 (R11A
529 and R11K) resulted in a less antimicrobial activity towards colistin-resistant *K. pneumoniae* and this
530 activity is rescued when testing mutants of colistin resistance modifying genes. These findings reinforce
531 our hypothesis that small changes to structure, not just the loss of the cystine residues can impact
532 antimicrobial acidity of protegrin-1 more than a +1-charge reduction.
533
534 To understand the changes in activity observed with the synthesized peptide variants, we investigated
535 their interactions with the outer and inner bacterial membrane. Outer membrane permeability
536 accounted for some of our activity changes as both our double variants exhibited higher fluorescence

537 compared to the parent peptide, suggesting they are getting stuck within the outer membrane **(Figure**
538 **5A)**. This is in line with what has been shown with polymyxin B nonapeptide lacking the lipid tail that
539 can still increase penetration through the outer membrane without inner membrane lysis [83]. The
540 differences in antimicrobial activity between our single proline peptide variants (R9P and R11P)
541 correlated will with inner membrane permeability. We found R9P peptide variant exhibited a slower
542 accumulation of inner membrane leakage compared to R11P, which behaved similarly to the parent
543 peptide **(Figure 7A),** revealing changes in pore formation ability may be the reason for the decrease in
544 antimicrobial activity with the R9P peptide variant. These findings reveal the small changes to protegrin-
545 1 structure, not just the major changes observed with cysteine bond removal [62], can impact inner
546 membrane leakage of the colistin-resistant *K. pneumoniae* membrane.
547
548 At the inner membrane protegrin-1 forms octameric pores, which cause cytoplasmic leakage [55].To
549 understand why our peptide variants behaved differently at the inner membrane we modeled our
550 variants as octameric pores. The resulting hypothetical models show a reduction in pore diameter and
551 visual pore collapse in both beta sheet peptide variants (R9P and R9P, R10L) **(Figure 8B and 8D)** but
552 not with our beta turn peptide variants (R11P and R10L, R11P) **(Figure 8C and 8E)**, where we found
553 they maintain pore integrity and diameter, only changing in peptide orientation within the pore. To
554 understand the structural instabilities leading to decreased pore formation we used GROMACs to
555 observe changes in the secondary structure in physiological salt conditions and within a lipid
556 environment. When assessing monomeric structural changes within salt conditions, we found the R9P
557 beta sheet peptide variant loses beta sheet structure early in the simulation while the R11P beta turn
558 variant can maintain beta sheet structure halfway through the simulation **(Figure 8G and 8H)**. The
559 R9P, R10L beta sheet peptide variant exhibits a much lower beta sheet character throughout the
560 entirety of the simulation **(Figure 8I)**, while the R10L, R11P beta turn peptide variant behaves much like
561 R11P peptide variant **(Figure 8H and 8J)**. These differences in monomeric behavior allowed us to
562 hypothesize that perhaps pore formation is hindered depending on at what point a variant loses its beta

563 sheet character. When assessing the dimer formation and stability in both salt and lipid environments
564 we found overall the orientation of the dimer changes with all variants, where the parental peptide
565 dimerizes in parallel orientation and the variants in anti-parallel orientation. In all the peptides
566 maintained structural integrity in the lipid environment more than the salt environment even at the
567 beginning of the simulation (0 seconds) (**Figure 8K-8O**). Furthermore, we found only the parental
568 protegrin-1 dimer separated after 100 ns (**Figure 8K**). These factors suggest strong dimerization may
569 not be as important for pore formation with protegrin-1.
570
571 In conclusion, colistin and host defense peptides antimicrobial activity has been largely attributed to
572 charge, as peptides with a higher positive charge will be more attracted to the negatively charged
573 membrane. We show that with colistin-resistant *K. pneumoniae*, small changes in structure can impact
574 antimicrobial activity more than decreasing the peptide charge from +6 to +5. This work represents a
575 step towards understanding how to prevent activity loss due to colistin resistance membrane
576 modifications when designing therapeutics for *K. pneumoniae*.
577
578 **Acknowledgements**
579 This work is supported by the National Institutes of Health R00AI163295 to RMF; Cesar de la Fuente-
580 Nunez holds a Presidential Professorship at the University of Pennsylvania and acknowledges funding
581 from the Procter & Gamble Company, United Therapeutics, a BBRF Young Investigator Grant, the
582 Nemirovsky Prize, Penn Health-Tech Accelerator Award, and the Dean's Innovation Fund from the
583 Perelman School of Medicine at the University of Pennsylvania. Research reported in this publication
584 was supported by the Langer Prize (AIChE Foundation), the National Institute of General Medical
585 Sciences of the National Institutes of Health under award number R35GM138201, and the Defense
586 Threat Reduction Agency (DTRA; HDTRA11810041, HDTRA1-21-1-0014, and HDTRA1-23-1-0001).
587 We would like to thank Bryan Davies for his support and guidance on this work and Cory DuPais for
588 teaching Christina how to process the SLAY library from the Illumina sequencing reads.

589

590 **Declaration of Interests**

591 Cesar de la Fuente-Nunez provides consulting services to Invaio Sciences and is a member of the
592 Scientific Advisory Boards of Nowture S.L. and Phare Bio. The de la Fuente Lab has received research
593 funding or in-kind donations from United Therapeutics, Strata Manufacturing PJSC, and Procter &
594 Gamble, none of which were used in support of this work. Cesar de la Fuente-Nunez is on the Advisory
595 Board of *Cell Reports Physical Science*.

596

597 **Author Contributions**

598 R.M.F. conceived the idea and designed the experimentation. MRSN colistin MICs performed by H.M.
599 Initial library creation performed by N.R, J.R, and R.M.F. Library analysis and direct cloning
600 experiments performed by C.D. Antimicrobial activity assessments and membrane analyses performed
601 by S.A. and C.D. Molecular Dynamic simulations performed by C.d.l.F.-N. and R.K. Biorender and
602 AlphaFold images produced by C.D. Text was written by R.M.F and C.D, and edits were discussed with
603 C.d.l.F.-N., R.K. and J.R.

604

605 **Materials and Methods**

606

607 **Bacterial strains and peptides.**

608 All bacterial isolates used in this study are listed in **Supplemental Table S1**. The peptides used in this
609 study are listed in **Table 1** with their molecular weight, length, charge, and secondary structure.
610 Pretegrin-1 was ordered through Anaspec for the comparison to other host defense peptides in **Figure**
611 **2**. Arenicin and Bac7(1-35) were purchased from Novopro because they were unavailable through
612 Anaspec. For consistency with our synthesized variants, protegrin-1 parent and peptide variants were
613 ordered from Novopro at >90% purity (https://www.novoprolabs.com) for comparing antimicrobial

614 activity of amino acid substitutions. All peptides were resuspended in ultra-purified water at 10 mg mL^{-1}
615 and stored at -20 °C.
616
617 **Minimal inhibitory concentration assays**.
618 All minimal inhibitory concentration assays were performed using the broth dilution method in 96-well
619 plates with the peptides tested by serial diluting in 0.2% BSA 0.01% acetic acid solution [84]. Bacteria
620 were synchronized to mid-log phase and standardized to a final optical density 600nm (OD_{600}) of 0.001
621 in Mueller Hinton broth to yield ~$5x10^5$ CFU mL^{-1}. The assay incubated for 20 hours at 37 °C before
622 determining MICs. All MICs were performed in triplicate and repeated on separate days.
623
624 **RT-qPCR of *phoP* expression levels**
625 Each *K. pneumoniae* strain was grown overnight in LB broth. The following day each strain was
626 synchronized to exponential phase at 37°C for 3 hours. RNA was extracted after bacteria had been
627 synchronized for 3 hours at 37°C. Following hot phenol chloroform extraction previously described [50]
628 samples were resuspended in nuclease free H_20 and quantified by Nanodrop. RNA were aliquoted and
629 stored at -80 for RT-qPCR. Samples were reverse transcribed with SuperScript™ IV VILO™ Master
630 Mix (11756050, Invitrogen) following the manufacturer's instructions. RTqPCR was performed using
631 PowerUp™ SYBR™ Green Master Mix (A25742, Applied Biosystems) following the manufacturer's
632 instructions, and the QuantStudio 3 Real-Time PCR System (A28567, Applied Biosystems). Primers
633 were designed using Integrated DNA Technologies, Inc. (IDT)'s PrimerQuest tool (**Table S4**). Relative
634 expression levels were calculated using the 2-ΔΔCt method [49] with *rpoD* as housekeeping control.
635 Triplicate samples were used with error shown as ±SEM.
636
637 **Alpha Fold Images**

638 Images were initially prepared using Google Collab and this link
639 https://colab.research.google.com/github/sokrypton/ColabFold/blob/main/AlphaFold2.ipynb#scrollTo=1
640 1I8k--10q0C. Each sequence was input, and images were displayed using the ChimeraX visualizer.
641 Primary and secondary structures were overlayed and mutated amino acids are shown in red.
642
643 **Ramachandran Plot Generation**
644 Plots were generated by taking previously generated alpha fold files and displaying them with the
645 visualizing tool from UCSF chimera. Program can be accessed by utilizing this link
646 https://www.cgl.ucsf.edu/chimera/download.html. Plots were recolored and overlayed using Adobe
647 Photoshop.
648
649 **dmSLAY protegrin-1 analysis**
650 *dmSLAY creations and screening***.** The protegrin-1 deep mutational library was created as previously
651 described [60] and inserted into a tetracycline resistant pMMB67EH plasmid. The library was first
652 electroporated into *E. coli* C3020 and >150,000 colonies were collected. The library was then
653 transformed into *E. coli* SM10 λpir mating strain and >270,000 colonies were collected. Finally,
654 conjugation was used to introduce the library to *K. pneumoniae* MKP103 and ~200,000 colonies were
655 collected. Samples were frozen in glycerol stocks until library screening. Triplicate samples *K.*
656 *pneumoniae* MKP103 harboring the dmSLAY protegrin-1 library were thawed and back diluted to and
657 OD_{600} 0.1 and grown for one hour. The samples were then back diluted to OD_{600} 0.01 in 5 mL terrific
658 broth (tryptone, yeast, potassium phosphate dibasic, and glycerol) and triplicate samples were induced
659 with 0.05 mM IPTG or uninduced (0mM IPTG) for three hours shaking (220rpm) at 37 °C followed by,
660 bacterial population collection and subsequent plasmid extraction. Barcoded primers (Table S7) were
661 used for PCR of the triplicate induced and uninduced plasmid populations for amplification of the 240
662 bp amplicon for Illumina sequencing. One lane of Illumina MiSeq run was used for amplicon coverage

663 to allow for quantification and calculation of log2 fold change between the induced and uninduced
664 samples.
665
666 *Bioinformatic Analysis*. The next generation sequencing reads were process by having their forward
667 and reverse sequences merged together and adaptor sequences trimmed. For this we used a unique
668 modification of DESQ2, a package associated with R Studio, typically used to investigate the presence
669 of genes within a population. More specifically, we merged forward and reverse raw sequences from a
670 previously made protegrin-1 library, and adaptors were trimmed from both 5' and 3' end of the
671 sequence. Reads were counted and those occurring less than 50 times within the population were
672 removed from analysis to allow for the possibility of machine error. Translated DNA sequences were
673 then compared to the reads of the uninduced and induced populations using the Deseq2 package in R
674 studio. To allow for analysis of specifically those reads that did not kill the bacteria we eliminated reads
675 with a log 2-fold change below 0. From this data each amino acid mutation at each position in the total
676 sequence variants were counted to quantify their occurrence within the population of peptide variants.
677
678 **Direct Cloning of Peptide Variants**
679 Procedure adapted from previous methods [59]. Briefly, protegrin-1 parent plasmid was used as a
680 template for cloning via restriction enzymes on the broad host plasmid PMMB67EH with a tetracycline
681 resistance cassette. Sequences were cloned with peptide variant primers listed in **Table S5** with
682 homology to the tether sequence on the reverse primer. Restriction digestion was performed using
683 KpmI and SalI cut sites. Each peptide variant was then transformed into *E.coli C320* (NEB)
684 electrocompetent cells and sequence variants were confirmed by sanger sequencing. Plasmid was
685 extracted from *E. coli* using Qiagen mini-prep kit and electroporated into MKP103 for testing of
686 antimicrobial activity with IPTG induction.
687
688 **Surface display validation of mutations identified in library screen**

689 Growth curve procedure was adapted from previous methods [59]. Each *K. pneumoniae* strain with
690 plasmids harboring peptide variants and control plasmids listed in **Table S6**. were grown overnight in
691 LB broth and 1% glucose solution supplemented with 20µg/mL of tetracycline. The following day each
692 strain was synchronized to exponential phase at 37°C for 3 hours. At that time the strains were
693 standardized to an OD_{600} of 0.02. Bacterial strains were then added to culture tubes containing 2 mL
694 LB, 0.5 mM IPTG, and 20 µg mL^{-1} tetracycline and grown shaking (220rpm) at 37°C over the course of
695 4 hours. At 0, 1, 2, and 4 hours 100 µL was removed from each culture tube and added to 900µL of
696 1XPBS for 1:10 serial dilutions that were then plated on LB agar with 50 µg/mL tetracycline. All
697 experiments were plated in triplicate and incubated overnight at 37°C, and colony forming units per mL
698 (CFU mL^{-1}) was calculated with error reported as ±SEM.
699
700 **Outer Membrane Permeability**
701 Procedure adapted from previous methods [69-71] Each *K. pneumoniae* strain was grown overnight in
702 LB broth. The following day each strain was synchronized to exponential phase at 37°C for 3 hours.
703 The cells were harvested by centrifugation (3434 rcf for 10 min) washed twice with buffer A (5mM
704 HEPES, 5mM glucose, pH 7.2) and resuspended in buffer A to an OD_{600} = 0.1. Then 100 µL Buffer A
705 with 20 µM NPN was added to 1000 µL washed cells in a clear-bottom black walled 96-well plate.
706 Peptide was added to a final concentration of 64 µg/mL and fluorescence was monitored at an
707 excitation of 350nm and emission of 420nm for 30 minutes at 3-minute intervals. The read form the no
708 cell control wells were removed from each treated well to normalize for background. All assays were
709 performed in triplicate with error reported as ±SEM.
710
711 **Membrane Depolarization**
712 The procedure used was adapted from a previous method [77]. Briefly, each *K. pneumoniae* strain was
713 grown overnight in LB broth. The following day each strain was synchronized to exponential phase at
714 37°C for 3 hours. The cells were harvested by centrifugation (3434 rcf for 10 min) washed twice with

715 buffer A (5mM HEPES, 5mM glucose, pH 7.2) and resuspended in buffer A and 100mM KCl to an
716 OD_{600} = 0.1, along with 20mM DiSC3 dye. Bacteria was added to clear-bottom black walled 96-well
717 plate and standardized for 30 minutes monitoring the florescence changes using a Biotech Synergy H1
718 plate reader with fluorescence kinetic reads set with excitation of 622nm and emission of 670nm for 30
719 minutes at 2-minute intervals. Peptide was then added to a final concentration of 64 µg mL^{-1} and
720 fluorescence changes were monitored for 30 minutes at 2-minute intervals using excitation of 622nm
721 and emission of 670nm. All assays were performed in triplicate with error reported as ±SEM.
722

723 **Inner Membrane Leakage**

724 The procedure used was adapted from a previous method [77, 78]. Each *K. pneumoniae* strain was
725 grown overnight in LB broth. The following day each strain was synchronized to exponential phase at
726 37°C for 3 hours. The cells were harvested by centrifugation (3434 rcf for 10 min) washed once with
727 0.1M sodium phosphate buffer (26mM NaH_2PO_4, 77mM Na2HPO4, pH 7.4) and resuspended in 0.1M
728 sodium phosphate buffer to an OD_{600} = 0.1 along with 10mM ONPG. The peptide were then serially
729 diluted in sodium phosphate buffer in a clear-bottom walled black 96-well plate, bacteria were added,
730 and absorbance was read using a Biotech Synergy H1 plate reader at 410nm for 45 minutes with reads
731 set at 3-minute intervals.
732

733 **Molecular Dynamics Simulations**

734 GROMACs version 2025.0 located https://www.gromacs.org/index.html was used to perform the
735 analysis of the peptide variant monomers as well as dimers in both a saline medium (ionic strength:
736 0.15 M NaCl) and a general Gram-negative inner membrane environment located https://charmm-
737 gui.org/?doc=archive&lib=biomembrane. This analysis analyzed changes in peptide secondary
738 structure as well as fluctuations in center of mass and residue contacts with peptide variant dimers.
739 Snapshots of the peptide monomers were taken at 0ns, and peptide dimers were taken at 0 and 100ns
740 to all for visualization of structural changes in each subunit.

741

742 **Figure Legends**

743

744 **Figure 1. Multi-level analysis used to investigate how protegrin-1 can bypass colistin resistance**.
745 Our initial determination of MKP103 to have colistin-resistance yet has variable susceptibility to
746 peptides of different structural class was used to inform our deep mutation scanning utilizing a genetic
747 screening platform (bottom). We then investigate peptide variants mutated in different regions of the
748 triple arginine motif for changes in antimicrobial activity, disruption to both the outer and inner
749 membrane (middle). We ultimately use molecular modeling of peptides and octameric pores and
750 combine this with molecular dynamic simulations to assess peptide structure stability (top). Octameric,
751 dimeric and monomeric models were generated using Alpha Fold and Biorender was used for both
752 vector production and for the creation of the final figure.

753

754 **Figure 2. Host defense peptides do not equally bypass *K. pneumoniae* MKP103 PhoP acquired**
755 **polymyxin resistance**. This figure shows bacteria and peptide screening to determine ideal candidates
756 to investigate colistin resistance. Colistin and polymyxin B MICs against drug-resistant *K. pneumoniae*
757 MKP103, hypervirulent *K. pneumoniae* NTUH and KPPR1S, drug-resistant *K. pneumoniae* ATCC
758 700603, and type strain *K. pneumoniae* ATCC 13883 (bars) overlayed with the baseline *phoP*
759 expression in exponential growth phase, normalized to housekeeping gene *rpoD* and graphed in
760 triplicate with error shown as ±SEM (**Figure 2A**). Fold change in MICs between the *K. pneumoniae*
761 MKP103 parental isolate and a *ΔphoP* transposon mutant (KPNIH1_10030-701::T30) of polymyxin B
762 (Poly-B), indolicidin (Indo), Melittin (Mel), Arenicin (Are), protegrin-1 (PG-1), and CecropinA (Cec A)
763 (**Figure 2B**). MIC assays were performed in triplicate for the data shown. **Figures 2C-2E** show the
764 Ramachandran plots depicting the psi and phi angles of alpha helical peptides, beta sheet peptides,
765 and extended/polyproline peptides, respectively.

766

767 **Figure 3. Protegrin-1 deep mutational scanning library shows reveals charge and structure are**
768 **important for antimicrobial activity towards colistin-resistant *K. pneumoniae* MKP103**. This figure
769 shows the results of the initial SLAY screening as well as validation with direct cloning. **Figure 3A** is a
770 heat Map of SLAY library analysis showing the number of occurrences of the amino acid mutations in
771 our Illumina sequencing populations retained with induction with the parent peptide sequence on the y
772 axis and possible mutations on the x axis. White boxes denote mutations outside of the defined
773 maximum range of the heat map (20 occurrences). **Figure 3B** shows the Alpha Fold representation of
774 protegrin-1 peptide with the mutations identified from the screen as outside of the defined maxima show
775 with their location highlighted in red and amino acid position number in parentheses. The amino acid
776 mutations denoted in blue text were cloned in the surface display system for validation by enumeration
777 of CFU mL^{-1} following IPTG plasmid induction over four hours with display of eighth the parent peptide
778 protegrin-1, uninduced plasmid control, and negative control 2xHA (**Figure 3C**) and peptide variants
779 (**Figure 3D**) identified in the screen. The surface display validation assays were performed in triplicate
780 with error shown.as as $\pm$SEM.

781

782 **Figure 4. The arginine to proline mutation impedes antimicrobial activity only in the beta-sheet**
783 **to turn transition region of the protegrin-1 arginine loop.** The figures show MICs (μmol L^{-1}) of
784 synthesized peptide variants and fold-change in MICs between colistin-resistant *K. pneumoniae*
785 MKP103 and transposon mutants lacking important LPS modifying genes. **Figure 4A** shows
786 synthesized peptide variants were tested against five colistin resistant clinical isolates. **Figure 4B**
787 shows the fold change of peptide MICs between the parental MKP103 and the *ΔphoP, ΔpagP, ΔpagL,*
788 *ΔarnT,* and *ΔpmrB* transposon mutants (mut/WT). Figure 4C and 4D shows the alanine and lysine
789 peptide variants MICs against the five colistin resistant clinical isolates and the fold change MICs

790 between the parental MKP103 and transposon mutants. Lines are drawn on figures 4B and 4C follow
791 the protegrin-1 parental peptide fold-change in MIC for *ΔphoP* (blue) and downstream genetic mutants
792 (red). Peptides were all tested at a maximum concentration of 31 μmol L^{-1}. MIC assays were performed
793 in triplicate for the data shown.

794

795 **Figure 5. Protegrin-1 double mutant variants with reduced charge display greater disruption of**
796 **colistin-resistant outer membrane.** Outer membrane fluorescence was monitored over 30 minutes
797 with peptide variants and controls carbenicillin and polymyxin B. **Figure 5A** shows *K. pneumoniae*
798 MKP103 normalized NPN fluorescence after treatment with single peptide variants and Figure 5B
799 shows the double peptide variants. The NPN fluorescence for the *ΔphoP* transposon mutant is shown
800 for peptide variants in **Figures 5C and 5D**. Endpoint fluorescence reads with single peptide variant
801 mutants with top five colistin resistant MRSN isolates, parental MKP103, *ΔphoP, ΔpagP, ΔpagL, ΔarnT,*
802 *and ΔpmrB* transposon mutants is shown on **Figure 5E**, and double peptide variant mutants on **Figure**
803 **5F**. All peptides and controls were tested in triplicate at a concentration of 31 μmol L^{-1} with error shown
804 as ±SEM.

805

806 **Figure 6. The arginine to proline mutation in the beta-sheet transition shows increased**
807 **membrane depolarization.** Membrane depolarization shows less active single peptide variant (R9P)
808 depolarizing more effectively than our more active single peptide variant (R11P). *K. pneumoniae*
809 MKP103 tested with single peptide variants (A) and double peptide variants (B). *ΔphoP* transposon
810 mutant tested against single peptide variants (C) and double peptide variants (D). Peptides were tested
811 at a concentration of 31 μmol L^{-1} with error shown as ±SEM.

812 .

813

814 **Figure 7. The arginine to proline mutation in the beta-sheet transition limits cytosolic leakage in**
815 **single and double mutation variants.** Inner membrane leakage shows more active single peptide
816 variant (R11P) disrupting more effectively than our less active single peptide variants (R9P, R10L). *K.*
817 *pneumoniae* MKP103 tested with single peptide variants (A) and double peptide variants (B). *ΔphoP*
818 transposon mutant tested against single peptide variants (C) and double peptide variants (D). Peptides
819 were tested at a concentration of 31 μmol L^{-1} with error shown as ±SEM.

820

821 **Figure 8. Molecular modeling shows octameric pore collapse and loss of beta sheet character in**
822 **beta sheet peptide variants.** Peptide variants are shown modeled as octameric pores in **Figure 8A-**
823 **8E** using AlphaFold2 and visualized using ChimeraX for parent protegrin-1 (**A**), R9P (**B**), R11P (**C**),
824 RR910PL (**D**) and RR1011LP (**E**). Amino acid sequences were aligned in the N to C termini direction.
825 **Figures 8F-8J** show monomeric peptide variants simulated using GROMACs and observed for
826 changes in secondary structure parent protegrin-1 (**F**), R9P (**G**), R11P (b), R9P, R10L (**I**) and R10L,
827 R11P (**J**). The heat map labels show the color coding for B = Beta Bridge, T =Turn, E = Extended
828 Conformation, C = Coil peptide structural components. **Figures 8K-8O** show dimeric peptide variants
829 simulated using GROMACs in both a salt box (0.15M NaCl at 310K) (top) and a general Gram-negative
830 inner membrane (bottom). Snapshots are shown for parent protegrin-1 (**K**), R9P (**L**), R11P (**M**), R9P,
831 R10L (**N**) and R10L, R11P (**O**) at 0 and 100ns for both simulated environments.

832

833 **Tables.**

834 **Table 1. Host defense peptides tested for antimicrobial activity towards *K. pneumoniae* MKP103**
835 **and MKP103 *ΔphoP* mutant.**
836

Name	AA sequence	MW (g/mol)	Charge	Secondary structure
Il-37[a]	LLGDFFRKSKEKIGKEFKRIVQRIKDFLRNLVPRTES	4492.34	+6	Alpha helix
Indolicidin[a]	ILPWKWPWWPWRR - NH2	1906.28	+4	extended
Protegrin-1[a]	RGGRLCYCRRRFCVCVGR - NH2	2003.48	+6	Beta sheet
Arenicin[b]	RWCVYAYVRVRGVLVRYRRCW-OH	2758.2	+6	Beta sheet
Cecropin[a]	KWKLFKKIEKVGQNIRDGIIKAGPAVAVVGQATQIAK-NH2	4004.10	+7	Alpha helix
Melittin[a]	GIGAVLKVLTTGLPALISWIKRKRQQ-NH2	2846.7	+6	Alpha helix
Bac7 (1-35)[b]	RRIRPRPPRLPRPRPRPLPFPRPGPRPIPRPLPFP-NH2	4206.16	+11	polyproline

837
838 [a] Peptide ordered from Anaspec
839 [b] Peptide ordered from Novopro

840 **Table 2. Occurrence of amino acid mutations in the peptide variant sequences lacking**
841 **antimicrobial activity.**
842

Amino Acid Mutation	Amino Acid Class Change	Number of Occurrences
F12L	non-polar to non-polar	834
G2R	non-polar to positive-charge	316
R10L*	positive-charge to non-polar	299
R9P*	positive-charge to non-polar	295
L5I	non-polar to non-polar	218
C6S	non-polar to polar	35
C13S	non-polar to polar	27
C15R	non-polar to positive-charge	22
G3R	non-polar to positive-charge	21
F12Y	non-polar to polar	21

843 *Amino acid mutations found together in 89% occurrences
844
845

846 **Table 3. Synthesized Peptide Variants.**

Name	Amino Acid Sequence	MW (g/mol)	Charge
PG-1 parent	RGGRLCYCRRRFCVCVGR	2160.63	+6
R9P	RGGRLCYCPRRFCVCVGR	2101.56	+5
R10L	RGGRLCYCRLRFCVCVGR	2117.60	+5
R11P	RGGRLCYCRRPFCVCVGR	2101.56	+5
RR910PL	RGGRLCYCPLRFCVCVGR	2058.53	+4
RR1011LP	RGGRLCYCRLPFCVCVGR	2058.53	+4
R9A	RGGRLCYCARRFCVCVGR	2075.52	+5
R11A	RGGRLCYCRRAFCVCVGR	2075.52	+5
R9K	RGGRLCYCKRRFCVCVGR	2132.62	+6
R11K	RGGRLCYCRRKFCVCVGR	2132.62	+6

847
848
849

850 **Table 4. Minimum inhibitory concentration of protegrin-1 and peptide variants towards *K.***
851 ***pneumoniae* MKP103 and transposon mutants.**
852

Peptide Variant	MIC (μmol L^{-1} / μg mL^{-1})					
	MKP103 WT	***ΔphoP***	***ΔpagP***	***ΔpagL***	***ΔarnT***	***ΔpmrB***
PG-1 parent	3.70/8	0.12/0.25	3.70/8	3.70/8	3.70/8	3.70/8
R9P	15.23/32	0.48/1	15.23/32	15.23/32	15.23/32	15.23/32
R10L	15.11/32	1.89/4	15.11/32	15.11/32	7.56/16	7.56/16
R11P	3.81/8	0.95/2	0.95/2	0.95/2	1.90/4	1.90/4
RR1011LP	31.09/64	0.97/2	15.55/32	15.55/32	15.55/32	15.55/32
RR910PL	31.09/64	3.89/8	31.09/64	31.09/64	31.09/64	31.09/64
R9A	15.41/32	0.96/2	1.93/4	3.85/8	1.93/4	3.85/8
R11A	15.41/32	0.48/1	0.96/2	0.96/2	0.96/2	1.93/4
R9K	3.75/8	0.47/1	0.94/2	0.94/2	0.94/2	0.94/2
R11K	7.50/16	0.47/1	0.94/2	0.94/2	0.94/2	0.94/2

853

854 **References**

855 1. Paczosa, M.K. and J. Mecsas, *Klebsiella pneumoniae: Going on the Offense with a Strong*
856 *Defense.* Microbiol Mol Biol Rev, 2016. **80**(3): p. 629-61.
857 2. Asokan, S., et al., *Klebsiella pneumoniae: A growing threat in the era of antimicrobial resistance.*
858 The Microbe, 2025. **7**: p. 100333.
859 3. Navon-Venezia, S., K. Kondratyeva, and A. Carattoli, *Klebsiella pneumoniae: a major worldwide*
860 *source and shuttle for antibiotic resistance.* FEMS Microbiol Rev, 2017. **41**(3): p. 252-275.
861 4. Shah, A.A., et al., *Emerging challenges in Klebsiella pneumoniae: Antimicrobial resistance and*
862 *novel approach.* Microbial Pathogenesis, 2025. **202**: p. 107399.
863 5. Reynolds, D., et al., *The threat of multidrug-resistant/extensively drug-resistant Gram-negative*
864 *respiratory infections: another pandemic.* Eur Respir Rev, 2022. **31**(166).
865 6. Antimicrobial Resistance, C., *Global burden of bacterial antimicrobial resistance in 2019: a*
866 *systematic analysis.* Lancet, 2022. **399**(10325): p. 629-655.
867 7. Petrosillo, N., F. Taglietti, and G. Granata, *Treatment Options for Colistin Resistant Klebsiella*
868 *pneumoniae: Present and Future.* J Clin Med, 2019. **8**(7).
869 8. Wyres, K.L., M.M.C. Lam, and K.E. Holt, *Population genomics of Klebsiella pneumoniae.* Nat Rev
870 Microbiol, 2020. **18**(6): p. 344-359.
871 9. Sati, H., et al., *The WHO Bacterial Priority Pathogens List 2024: a prioritisation study to guide*
872 *research, development, and public health strategies against antimicrobial resistance.* Lancet
873 Infect Dis, 2025.
874 10. Mondal, A.H., et al., *A Review on Colistin Resistance: An Antibiotic of Last Resort.*
875 Microorganisms, 2024. **12**(4).
876 11. Rojas, L.J., et al., *Colistin Resistance in Carbapenem-Resistant Klebsiella pneumoniae:*
877 *Laboratory Detection and Impact on Mortality.* Clin Infect Dis, 2017. **64**(6): p. 711-718.
878 12. van Duin, D. and Y. Doi, *Outbreak of Colistin-Resistant, Carbapenemase-Producing Klebsiella*
879 *pneumoniae: Are We at the End of the Road?* J Clin Microbiol, 2015. **53**(10): p. 3116-7.
880 13. Luterbach, C.L., et al., *Transmission of Carbapenem-Resistant Klebsiella pneumoniae in US*
881 *Hospitals.* Clin Infect Dis, 2023. **76**(2): p. 229-237.
882 14. Horvath, M., et al., *Virulence Characteristics and Molecular Typing of Carbapenem-Resistant*
883 *ST15 Klebsiella pneumoniae Clinical Isolates, Possessing the K24 Capsular Type.* Antibiotics
884 (Basel), 2023. **12**(3).
885 15. Marsh, J.W., et al., *Evolution of Outbreak-Causing Carbapenem-Resistant Klebsiella pneumoniae*
886 *ST258 at a Tertiary Care Hospital over 8 Years.* mBio, 2019. **10**(5).
887 16. Chen, L., et al., *Epidemic Klebsiella pneumoniae ST258 Is a Hybrid Strain.* mBio, 2014. **5**(3): p.
888 10.1128/mbio.01355-14.
889 17. Bogdanovich, T., et al., *Colistin-resistant, Klebsiella pneumoniae carbapenemase (KPC)-*
890 *producing Klebsiella pneumoniae belonging to the international epidemic clone ST258.* Clin
891 Infect Dis, 2011. **53**(4): p. 373-6.
892 18. Lapp, Z., et al., *Fitness barriers to spread of colistin resistance overcome by first establishing*
893 *niche in patients with enhanced colistin exposure.* medRxiv, 2021: p. 2021.06.11.21258758.
894 19. Pitt, M.E., et al., *Octapeptin C4 and polymyxin resistance occur via distinct pathways in an*
895 *epidemic XDR Klebsiella pneumoniae ST258 isolate.* J Antimicrob Chemother, 2019. **74**(3): p.
896 582-593.

897 20. Arena, F., et al., *Colistin Resistance Caused by Inactivation of the MgrB Regulator Is Not*
898 *Associated with Decreased Virulence of Sequence Type 258 KPC Carbapenemase-Producing*
899 *Klebsiella pneumoniae.* Antimicrob Agents Chemother, 2016. **60**(4): p. 2509-12.
900 21. Diani, E., et al., *Colistin: Lights and Shadows of an Older Antibiotic.* Molecules, 2024. **29**(13).
901 22. Khondker, A. and M.C. Rheinstädter, *How do bacterial membranes resist polymyxin antibiotics?*
902 Communications Biology, 2020. **3**(1): p. 77.
903 23. Hamel, M., J.M. Rolain, and S.A. Baron, *The History of Colistin Resistance Mechanisms in*
904 *Bacteria: Progress and Challenges.* Microorganisms, 2021. **9**(2).
905 24. Yu, Z., et al., *Antibacterial mechanisms of polymyxin and bacterial resistance.* Biomed Res Int,
906 2015. **2015**: p. 679109.
907 25. Simpson, B.W. and M.S. Trent, *Pushing the envelope: LPS modifications and their consequences.*
908 Nat Rev Microbiol, 2019. **17**(7): p. 403-416.
909 26. Bray, A.S., et al., *MgrB-Dependent Colistin Resistance in Klebsiella pneumoniae Is Associated*
910 *with an Increase in Host-to-Host Transmission.* mBio, 2022. **13**(2): p. e03595-21.
911 27. Janssen, A.B., et al., *Evolution of Colistin Resistance in the Klebsiella pneumoniae Complex*
912 *Follows Multiple Evolutionary Trajectories with Variable Effects on Fitness and Virulence*
913 *Characteristics.* Antimicrob Agents Chemother, 2020. **65**(1).
914 28. Li, L., et al., *Roles of two-component regulatory systems in Klebsiella pneumoniae: Regulation of*
915 *virulence, antibiotic resistance, and stress responses.* Microbiol Res, 2023. **272**: p. 127374.
916 29. Kim, S.J., et al., *Roles of crrAB two-component regulatory system in Klebsiella pneumoniae:*
917 *growth yield, survival in initial colistin treatment stage, and virulence.* Int J Antimicrob Agents,
918 2024. **63**(1): p. 107011.
919 30. Arroyo Luis, A., et al., *The pmrCAB Operon Mediates Polymyxin Resistance in Acinetobacter*
920 *baumannii ATCC 17978 and Clinical Isolates through Phosphoethanolamine Modification of*
921 *Lipid A.* Antimicrobial Agents and Chemotherapy, 2011. **55**(8): p. 3743-3751.
922 31. Lee, K.K., et al., *Heterogeneous efflux pump expression underpins phenotypic resistance to*
923 *antimicrobial peptides*. 2024, eLife Sciences Publications, Ltd.
924 32. MacNair, C.R., et al., *Overcoming mcr-1 mediated colistin resistance with colistin in combination*
925 *with other antibiotics.* Nat Commun, 2018. **9**(1): p. 458.
926 33. Brogden, K.A., *Antimicrobial peptides: pore formers or metabolic inhibitors in bacteria?* Nat Rev
927 Microbiol, 2005. **3**(3): p. 238-50.
928 34. Sengupta, D., et al., *Toroidal pores formed by antimicrobial peptides show significant disorder.*
929 Biochimica et Biophysica Acta (BBA) - Biomembranes, 2008. **1778**(10): p. 2308-2317.
930 35. Zhang, Q.Y., et al., *Antimicrobial peptides: mechanism of action, activity and clinical potential.*
931 Mil Med Res, 2021. **8**(1): p. 48.
932 36. Hancock, R.E. and A. Rozek, *Role of membranes in the activities of antimicrobial cationic*
933 *peptides.* FEMS Microbiol Lett, 2002. **206**(2): p. 143-9.
934 37. Fleeman, R.M. and B.W. Davies, *Polyproline Peptide Aggregation with Klebsiella pneumoniae*
935 *Extracellular Polysaccharides Exposes Biofilm Associated Bacteria.* Microbiol Spectr, 2022. **10**(2):
936 p. e0202721.
937 38. Fleeman, R.M., et al., *Defining principles that influence antimicrobial peptide activity against*
938 *capsulated Klebsiella pneumoniae.* Proc Natl Acad Sci U S A, 2020. **117**(44): p. 27620-27626.
939 39. El-Sayed Ahmed, M.A.E., et al., *Colistin and its role in the Era of antibiotic resistance: an*
940 *extended review (2000-2019).* Emerg Microbes Infect, 2020. **9**(1): p. 868-885.

941 40. Lei, J., et al., *The antimicrobial peptides and their potential clinical applications.* Am J Transl Res,
942 2019. **11**(7): p. 3919-3931.
943 41. Drayton, M., et al., *Host Defense Peptides: Dual Antimicrobial and Immunomodulatory Action.*
944 Int J Mol Sci, 2021. **22**(20).
945 42. Bader, M.W., et al., *Recognition of Antimicrobial Peptides by a Bacterial Sensor Kinase.* Cell,
946 2005. **122**(3): p. 461-472.
947 43. Wu, K.-M., et al., *Genome Sequencing and Comparative Analysis of Klebsiella pneumoniae*
948 *NTUH-K2044, a Strain Causing Liver Abscess and Meningitis.* Journal of Bacteriology, 2009.
949 **191**(14): p. 4492-4501.
950 44. Walker Kimberly, A., et al., *A Klebsiella pneumoniae Regulatory Mutant Has Reduced Capsule*
951 *Expression but Retains Hypermucoviscosity.* mBio, 2019. **10**(2): p. 10.1128/mbio.00089-19.
952 45. Rasheed, J.K., et al., *Characterization of the Extended-Spectrum β-Lactamase Reference Strain,*
953 *Klebsiella pneumoniae K6 (ATCC 700603), Which Produces the Novel Enzyme SHV-18.*
954 Antimicrobial Agents and Chemotherapy, 2000. **44**(9): p. 2382-2388.
955 46. Cowan, S.T., et al., *A classification of the Klebsiella group.* J Gen Microbiol, 1960. **23**: p. 601-12.
956 47. Ramage, B., et al., *Comprehensive Arrayed Transposon Mutant Library of Klebsiella pneumoniae*
957 *Outbreak Strain KPNIH1.* J Bacteriol, 2017. **199**(20).
958 48. Snitkin, E.S., et al., *Tracking a hospital outbreak of carbapenem-resistant Klebsiella pneumoniae*
959 *with whole-genome sequencing.* Sci Transl Med, 2012. **4**(148): p. 148ra116.
960 49. Livak, K.J. and T.D. Schmittgen, *Analysis of relative gene expression data using real-time*
961 *quantitative PCR and the 2(-Delta Delta C(T)) Method.* Methods, 2001. **25**(4): p. 402-8.
962 50. Aiba, H., S. Adhya, and B. de Crombrugghe, *Evidence for two functional gal promoters in intact*
963 *Escherichia coli cells.* J Biol Chem, 1981. **256**(22): p. 11905-10.
964 51. Mardirossian, M., et al., *The Host Antimicrobial Peptide Bac71-35 Binds to Bacterial Ribosomal*
965 *Proteins and Inhibits Protein Synthesis.* Chemistry & Biology, 2014. **21**(12): p. 1639-1647.
966 52. Barlow, D.J. and J.M. Thornton, *Helix geometry in proteins.* Journal of Molecular Biology, 1988.
967 **201**(3): p. 601-619.
968 53. Hauser, K., et al., *Characterization of Biomolecular Helices and Their Complementarity Using*
969 *Geometric Analysis.* J Chem Inf Model, 2017. **57**(4): p. 864-874.
970 54. Hollingsworth, S.A. and P.A. Karplus, *A fresh look at the Ramachandran plot and the occurrence*
971 *of standard structures in proteins.* Biomol Concepts, 2010. **1**(3-4): p. 271-283.
972 55. Bolintineanu, D.S., V. Vivcharuk, and Y.N. Kaznessis, *Multiscale models of the antimicrobial*
973 *peptide protegrin-1 on gram-negative bacteria membranes.* Int J Mol Sci, 2012. **13**(9): p. 11000-
974 11011.
975 56. Fahrner, R.L., et al., *Solution structure of protegrin-1, a broad-spectrum antimicrobial peptide*
976 *from porcine leukocytes.* Chem Biol, 1996. **3**(7): p. 543-50.
977 57. Steinberg, D.A., et al., *Protegrin-1: a broad-spectrum, rapidly microbicidal peptide with in vivo*
978 *activity.* Antimicrob Agents Chemother, 1997. **41**(8): p. 1738-42.
979 58. Tachi, Y., S.G. Itoh, and H. Okumura, *Molecular dynamics simulations of amyloid-beta peptides*
980 *in heterogeneous environments.* Biophys Physicobiol, 2022. **19**: p. 1-18.
981 59. Tucker, A.T., et al., *Discovery of Next-Generation Antimicrobials through Bacterial Self-Screening*
982 *of Surface-Displayed Peptide Libraries.* Cell, 2018. **172**(3): p. 618-628 e13.
983 60. Randall, J.R., et al., *Deep mutational scanning and machine learning uncover antimicrobial*
984 *peptide features driving membrane selectivity.* Res Sq, 2023.

985 61. Rodziewicz-Motowidlo, S., et al., *Antimicrobial and conformational studies of the active and*
986 *inactive analogues of the protegrin-1 peptide.* FEBS J, 2010. **277**(4): p. 1010-22.
987 62. Mohanram, H. and S. Bhattacharjya, *Cysteine deleted protegrin-1 (CDP-1): Anti-bacterial*
988 *activity, outer-membrane disruption and selectivity.* Biochimica et Biophysica Acta (BBA) -
989 General Subjects, 2014. **1840**(10): p. 3006-3016.
990 63. Martin, M.J., et al., *A panel of diverse Klebsiella pneumoniae clinical isolates for research and*
991 *development.* Microb Genom, 2023. **9**(5).
992 64. Bishop, R.E., *The lipid A palmitoyltransferase PagP: molecular mechanisms and role in bacterial*
993 *pathogenesis.* Mol Microbiol, 2005. **57**(4): p. 900-12.
994 65. Brett, P.J., D. DeShazer, and D.E. Woods, *Burkholderia thailandensis sp. nov., a Burkholderia*
995 *pseudomallei-like species.* Int J Syst Bacteriol, 1998. **48 Pt 1**: p. 317-20.
996 66. Jacobs Anna, C., et al., *AB5075, a Highly Virulent Isolate of Acinetobacter baumannii, as a Model*
997 *Strain for the Evaluation of Pathogenesis and Antimicrobial Treatments.* mBio, 2014. **5**(3): p.
998 10.1128/mbio.01076-14.
999 67. Jensen, K.F., *The Escherichia coli K-12 "wild types" W3110 and MG1655 have an rph frameshift*
1000 *mutation that leads to pyrimidine starvation due to low pyrE expression levels.* J Bacteriol, 1993.
1001 **175**(11): p. 3401-7.
1002 68. Minogue, T.D., et al., *Complete Genome Assembly of Escherichia coli ATCC 25922, a Serotype O6*
1003 *Reference Strain.* Genome Announc, 2014. **2**(5).
1004 69. Loh, B., C. Grant, and R.E. Hancock, *Use of the fluorescent probe 1-N-phenylnaphthylamine to*
1005 *study the interactions of aminoglycoside antibiotics with the outer membrane of Pseudomonas*
1006 *aeruginosa.* Antimicrob Agents Chemother, 1984. **26**(4): p. 546-51.
1007 70. Muheim, C., et al., *Increasing the permeability of Escherichia coli using MAC13243.* Sci Rep,
1008 2017. **7**(1): p. 17629.
1009 71. Richard, C.S.M., et al., *Outer Membrane Integrity-Dependent Fluorescence of the Japanese Eel*
1010 *UnaG Protein in Live Escherichia coli Cells.* Biosensors (Basel), 2023. **13**(2).
1011 72. Rizzetto, G., et al., *Protegrin-1 and Analogues Against Acinetobacter baumannii: A Narrative*
1012 *Review.* Pharmaceuticals (Basel), 2025. **18**(3).
1013 73. Huang, H.W., *DAPTOMYCIN, its membrane-active mechanism vs. that of other antimicrobial*
1014 *peptides.* Biochimica et Biophysica Acta (BBA) - Biomembranes, 2020. **1862**(10): p. 183395.
1015 74. Spindler, E.C., et al., *Deciphering the mode of action of the synthetic antimicrobial peptide*
1016 *Bac8c.* Antimicrob Agents Chemother, 2011. **55**(4): p. 1706-16.
1017 75. Mihaylova-Garnizova, R., et al., *Antimicrobial Peptides Derived from Bacteria: Classification,*
1018 *Sources, and Mechanism of Action against Multidrug-Resistant Bacteria.* Int J Mol Sci, 2024.
1019 **25**(19).
1020 76. Xiao, B., et al., *Unlocking the Potential of Antimicrobial Peptides: Cutting-Edge Advances and*
1021 *Therapeutic Potential in Combating Bacterial Keratitis.* Bioconjug Chem, 2025. **36**(3): p. 311-
1022 331.
1023 77. Moller, A.M., et al., *Common and varied molecular responses of Escherichia coli to five different*
1024 *inhibitors of the lipopolysaccharide biosynthetic enzyme LpxC.* J Biol Chem, 2024. **300**(4): p.
1025 107143.
1026 78. Gravel, J., C. Paradis-Bleau, and A.R. Schmitzer, *Adaptation of a bacterial membrane*
1027 *permeabilization assay for quantitative evaluation of benzalkonium chloride as a membrane-*
1028 *disrupting agent.* MedChemComm, 2017. **8**(7): p. 1408-1413.

1029 79. Nielsen, J.E., et al., *Self-Assembly of Antimicrobial Peptoids Impacts Their Biological Effects on*
1030 *ESKAPE Bacterial Pathogens.* ACS Infect Dis, 2022. **8**(3): p. 533-545.
1031 80. Ferreira, A.F.L., et al., *Defensins identified through molecular de-extinction.* Cell Reports Physical
1032 Science, 2024. **5**(9): p. 102193.
1033 81. Pogozheva, I.D., et al., *Comparative Molecular Dynamics Simulation Studies of Realistic*
1034 *Eukaryotic, Prokaryotic, and Archaeal Membranes.* J Chem Inf Model, 2022. **62**(4): p. 1036-
1035 1051.
1036 82. Saxena, D., et al., *Tackling the outer membrane: facilitating compound entry into Gram-*
1037 *negative bacterial pathogens.* npj Antimicrobials and Resistance, 2023. **1**(1): p. 17.
1038 83. Trimble, M.J., et al., *Polymyxin: Alternative Mechanisms of Action and Resistance.* Cold Spring
1039 Harb Perspect Med, 2016. **6**(10).
1040 84. Wiegand, I., K. Hilpert, and R.E.W. Hancock, *Agar and broth dilution methods to determine the*
1041 *minimal inhibitory concentration (MIC) of antimicrobial substances.* Nature Protocols, 2008.
1042 **3**(2): p. 163-175.
1043
1044

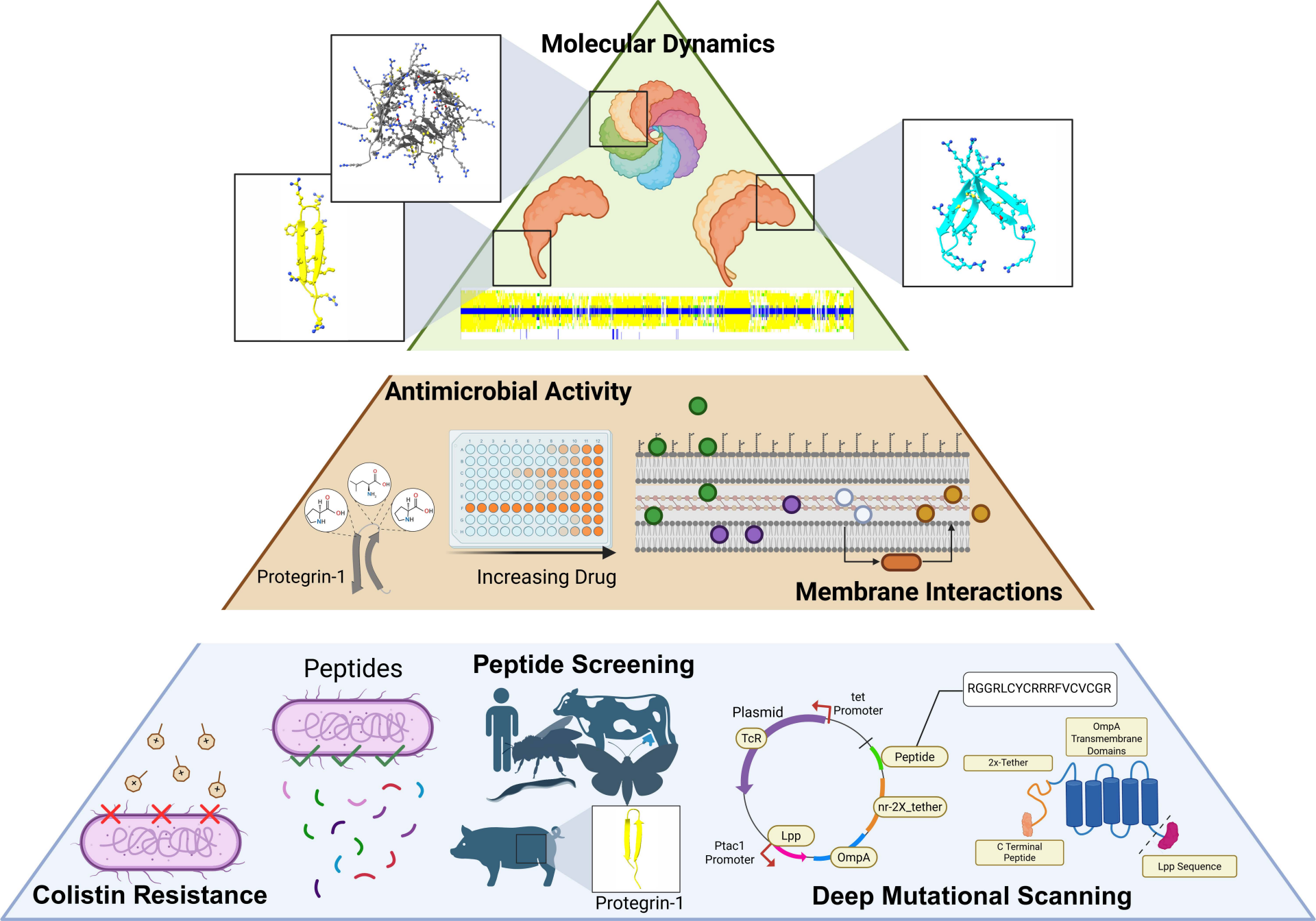
Molecular Dynamics
Antimicrobial Activity
Protegrin-1
Increasing Drug
Membrane Interactions
Peptides
Peptide Screening
Colistin Resistance
Protegrin-1
Plasmid
tet
Promoter
TcR
Peptide
nr-2X_tether
Lpp
OmpA
Ptac1
Promoter
RGGRLCYCRRRFVCVCGR
OmpA
Transmembrane
Domains
2x-Tether
C Terminal
Peptide
Lpp Sequence
Deep Mutational Scanning

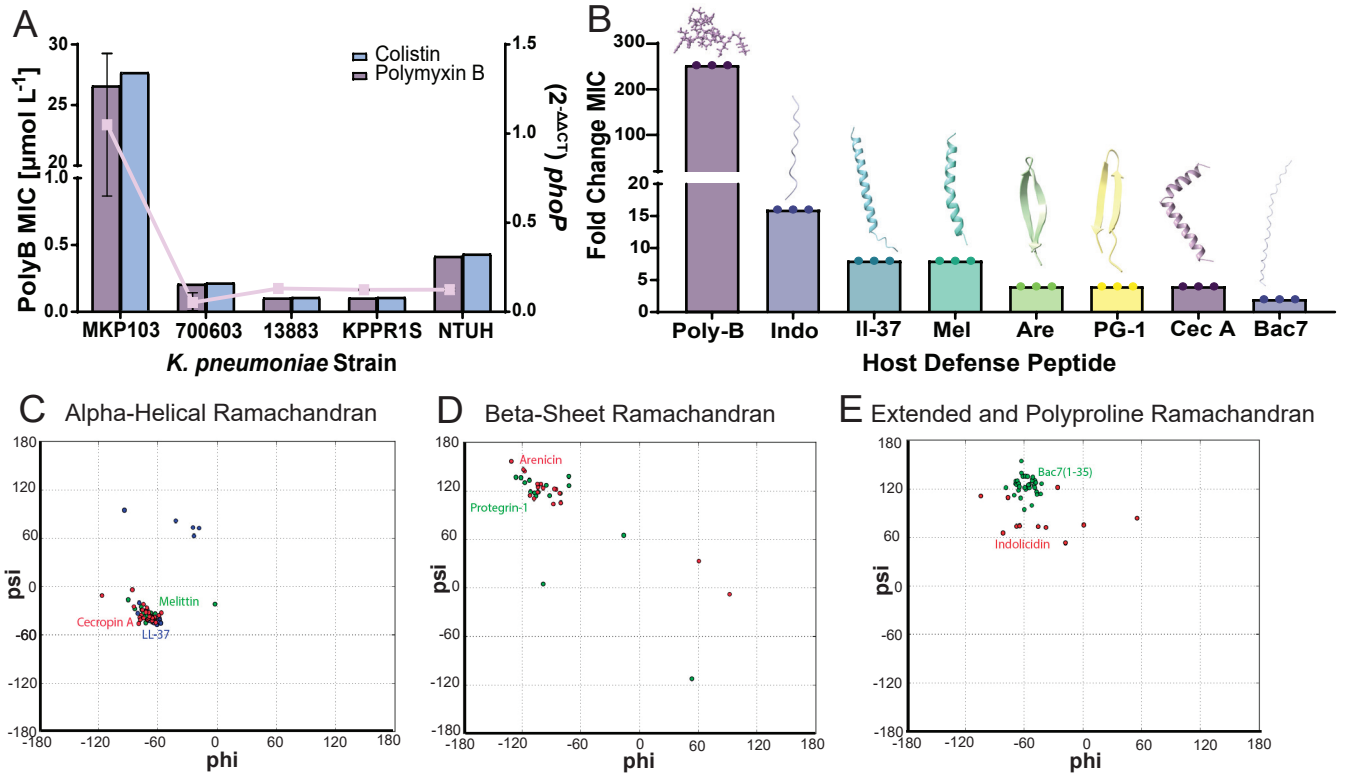
A
Colistin
Polymyxin B
PolyB MIC [μmol L-1]
(2-ΔΔCT) phoP
MKP103
700603
13883
KPPR1S
NTUH
K. pneumoniae Strain
B
Fold Change MIC
Poly-B
Indo
Il-37
Mel
Are
PG-1
Cec A
Bac7
Host Defense Peptide
C Alpha-Helical Ramachandran
Melittin
Cecropin A
LL-37
psi
phi
D Beta-Sheet Ramachandran
Arenicin
Protegrin-1
psi
phi
E Extended and Polyproline Ramachandran
Bac7(1-35)
Indolicidin
psi
phi

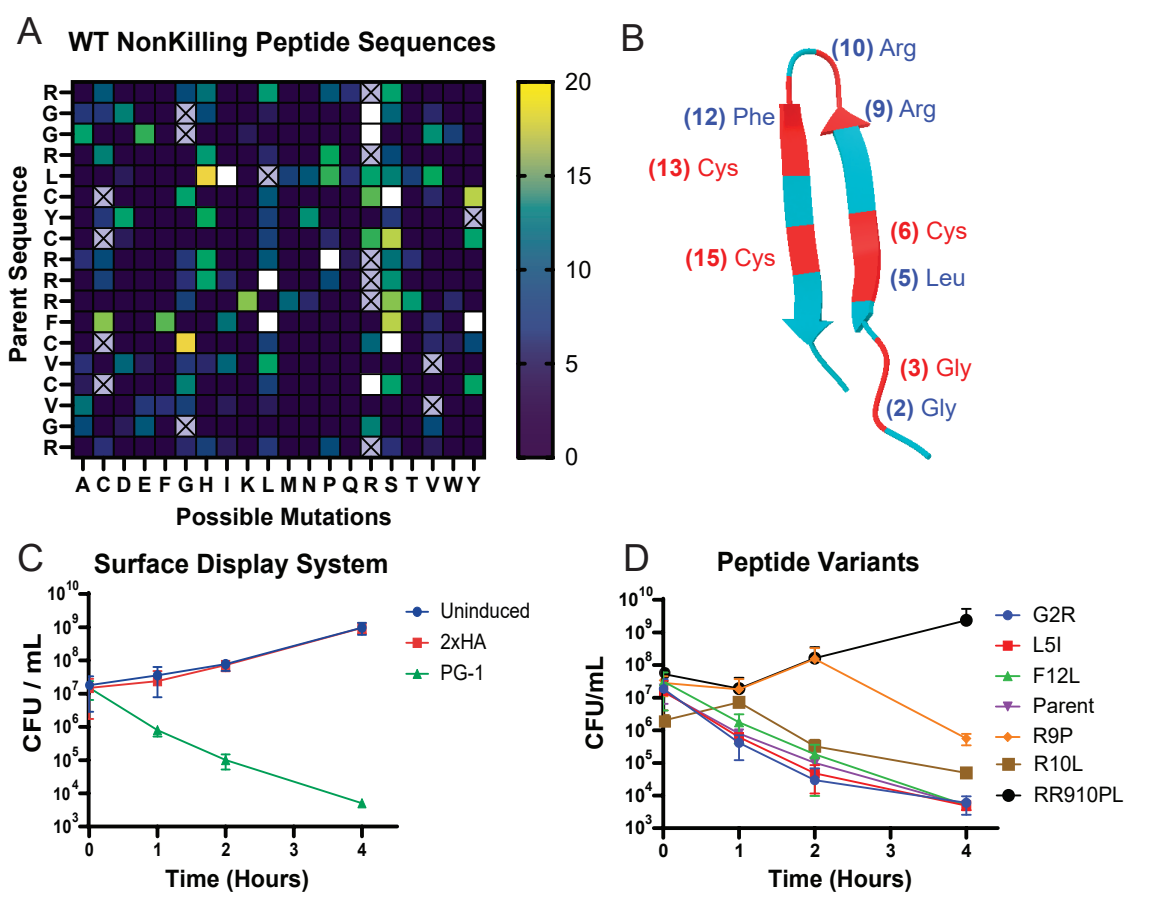
A
WT NonKilling Peptide Sequences
Parent Sequence
R G G R L C Y C R R R F C V C V G R
A C D E F G H I K L M N P Q R S T V W Y
Possible Mutations
20
15
10
5
0
B
(10) Arg
(9) Arg
(12) Phe
(13) Cys
(6) Cys
(15) Cys
(5) Leu
(3) Gly
(2) Gly
C
Surface Display System
CFU / mL
Time (Hours)
Uninduced
2xHA
PG-1
D
Peptide Variants
CFU/mL
Time (Hours)
G2R
L5I
F12L
Parent
R9P
R10L
RR910PL

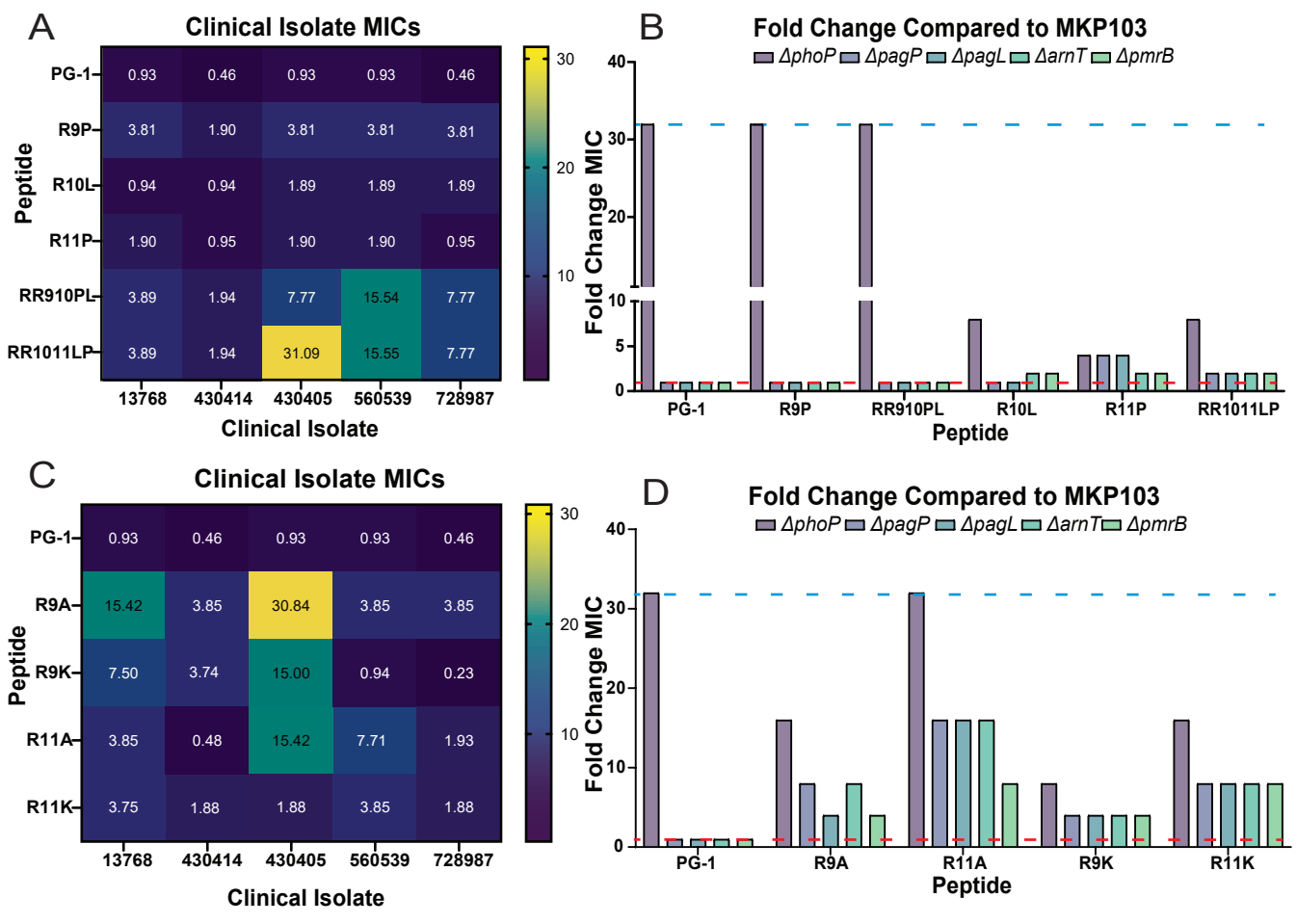
A
Clinical Isolate MICs
Peptide
PG-1
R9P
R10L
R11P
RR910PL
RR1011LP
0.93 0.46 0.93 0.93 0.46
3.81 1.90 3.81 3.81 3.81
0.94 0.94 1.89 1.89 1.89
1.90 0.95 1.90 1.90 0.95
3.89 1.94 7.77 15.54 7.77
3.89 1.94 31.09 15.55 7.77
13768 430414 430405 560539 728987
Clinical Isolate
30
20
10
B
Fold Change Compared to MKP103
ΔphoP ΔpagP ΔpagL ΔarnT ΔpmrB
Fold Change MIC
40
30
20
10
5
0
PG-1 R9P RR910PL R10L R11P RR1011LP
Peptide
C
Clinical Isolate MICs
Peptide
PG-1
R9A
R9K
R11A
R11K
0.93 0.46 0.93 0.93 0.46
15.42 3.85 30.84 3.85 3.85
7.50 3.74 15.00 0.94 0.23
3.85 0.48 15.42 7.71 1.93
3.75 1.88 1.88 3.85 1.88
13768 430414 430405 560539 728987
Clinical Isolate
30
20
10
D
Fold Change Compared to MKP103
ΔphoP ΔpagP ΔpagL ΔarnT ΔpmrB
Fold Change MIC
40
30
20
10
0
PG-1 R9A R11A R9K R11K
Peptide

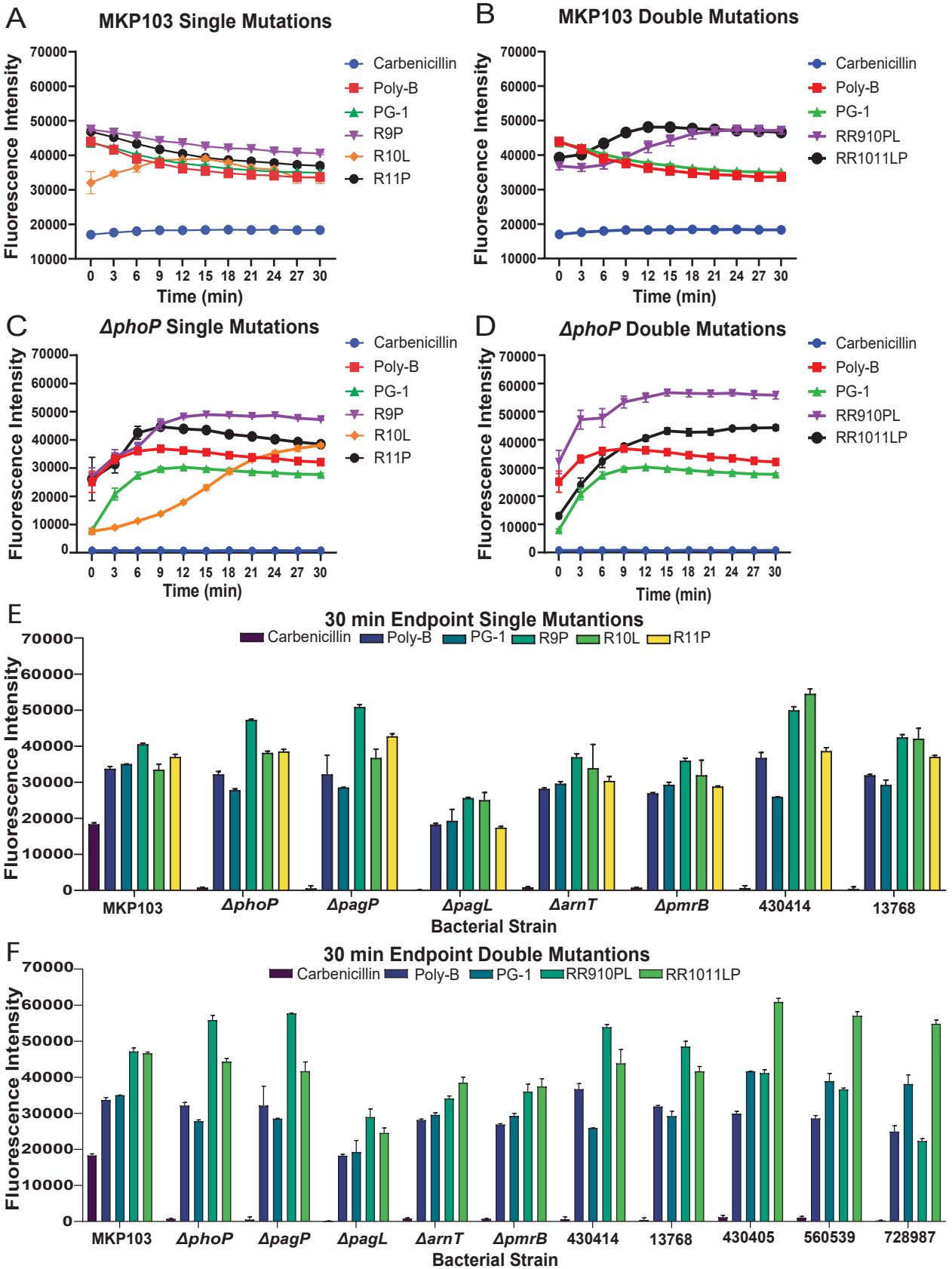
A
MKP103 Single Mutations
Fluorescence Intensity
Time (min)
Carbenicillin
Poly-B
PG-1
R9P
R10L
R11P
B
MKP103 Double Mutations
Fluorescence Intensity
Time (min)
Carbenicillin
Poly-B
PG-1
RR910PL
RR1011LP
C
ΔphoP Single Mutations
Fluorescence Intensity
Time (min)
Carbenicillin
Poly-B
PG-1
R9P
R10L
R11P
D
ΔphoP Double Mutations
Fluorescence Intensity
Time (min)
Carbenicillin
Poly-B
PG-1
RR910PL
RR1011LP
E
30 min Endpoint Single Mutantions
Carbenicillin
Poly-B
PG-1
R9P
R10L
R11P
Fluorescence Intensity
MKP103
ΔphoP
ΔpagP
ΔpagL
ΔarnT
ΔpmrB
430414
13768
Bacterial Strain
F
30 min Endpoint Double Mutantions
Carbenicillin
Poly-B
PG-1
RR910PL
RR1011LP
Fluorescence Intensity
MKP103
ΔphoP
ΔpagP
ΔpagL
ΔarnT
ΔpmrB
430414
13768
430405
560539
728987
Bacterial Strain

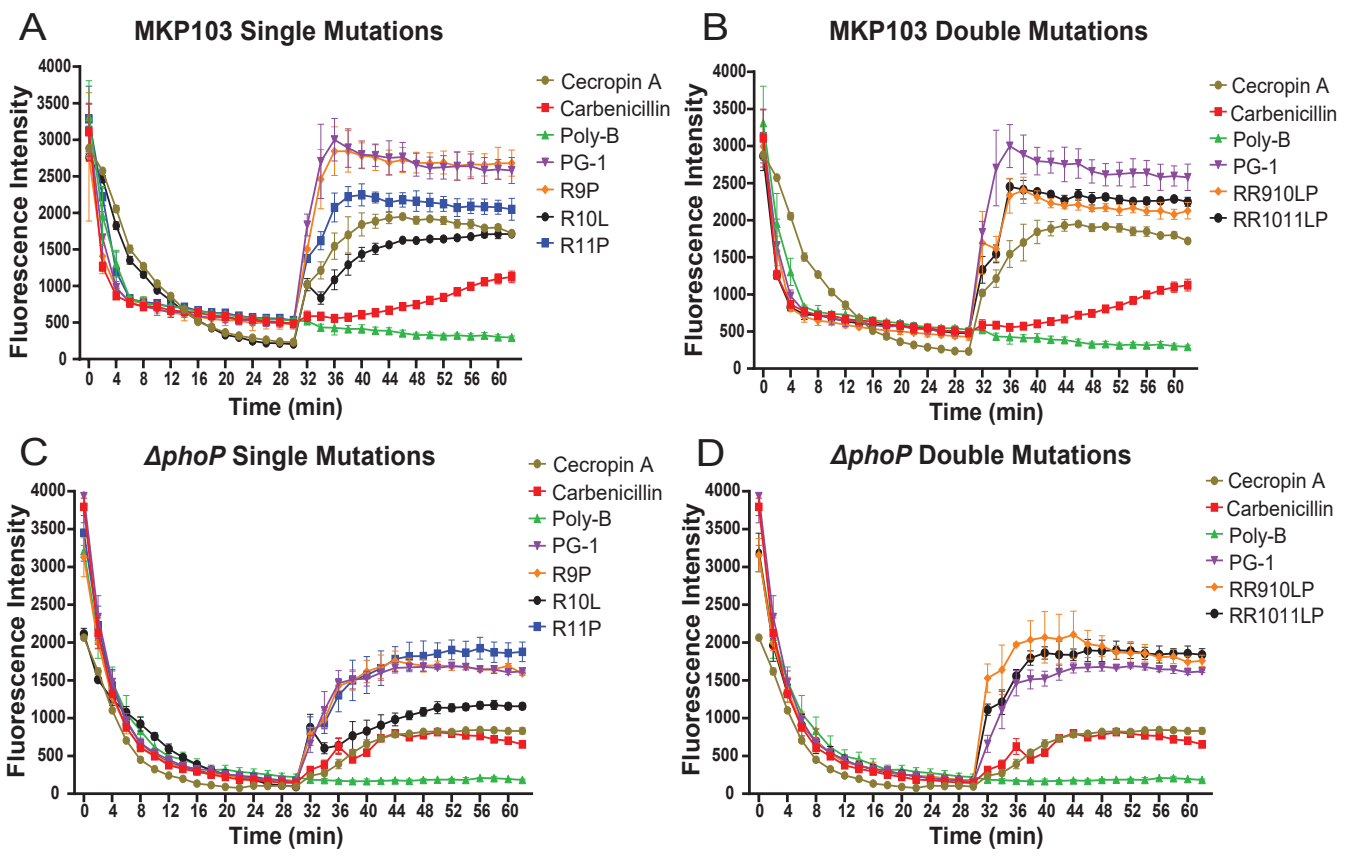
A
MKP103 Single Mutations
Fluorescence Intensity
Time (min)
Cecropin A
Carbenicillin
Poly-B
PG-1
R9P
R10L
R11P
B
MKP103 Double Mutations
Fluorescence Intensity
Time (min)
Cecropin A
Carbenicillin
Poly-B
PG-1
RR910LP
RR1011LP
C
ΔphoP Single Mutations
Fluorescence Intensity
Time (min)
Cecropin A
Carbenicillin
Poly-B
PG-1
R9P
R10L
R11P
D
ΔphoP Double Mutations
Fluorescence Intensity
Time (min)
Cecropin A
Carbenicillin
Poly-B
PG-1
RR910LP
RR1011LP

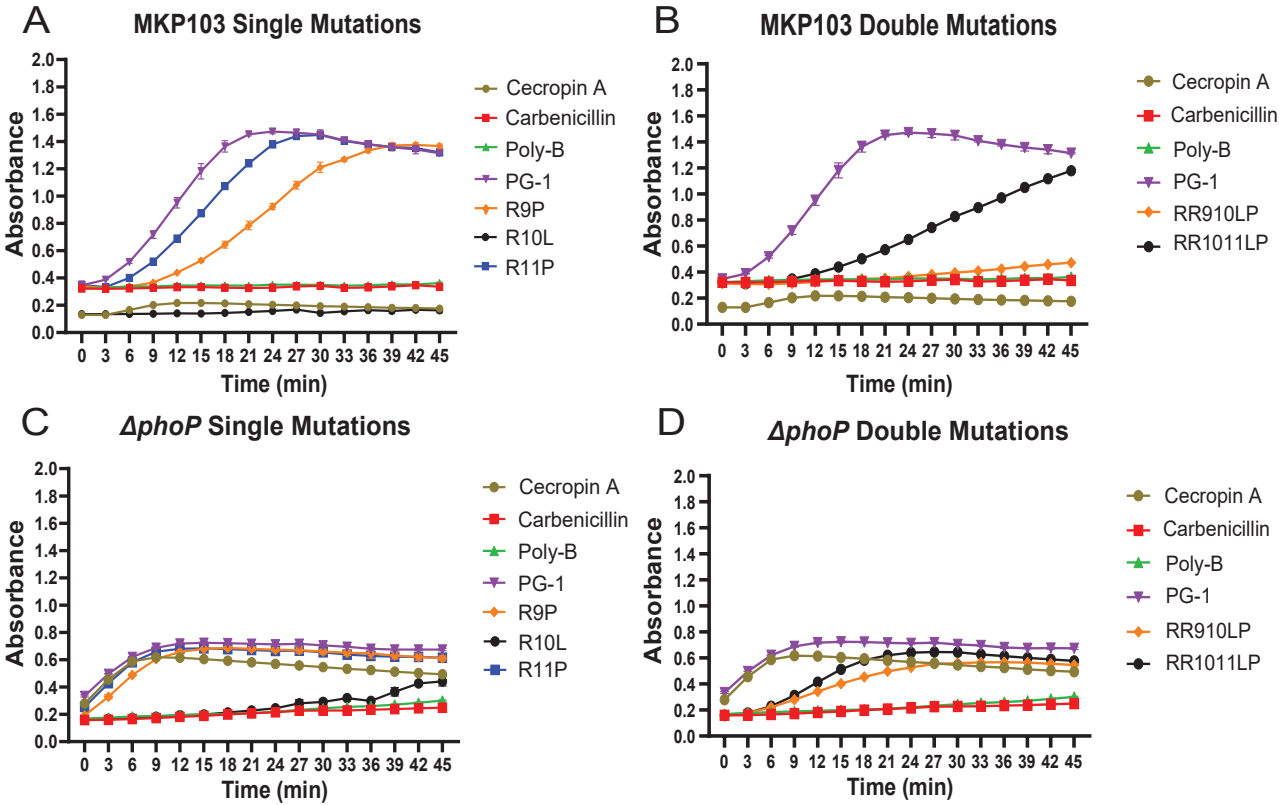
A
MKP103 Single Mutations
Absorbance
Time (min)
Cecropin A
Carbenicillin
Poly-B
PG-1
R9P
R10L
R11P
B
MKP103 Double Mutations
Absorbance
Time (min)
Cecropin A
Carbenicillin
Poly-B
PG-1
RR910LP
RR1011LP
C
ΔphoP Single Mutations
Absorbance
Time (min)
Cecropin A
Carbenicillin
Poly-B
PG-1
R9P
R10L
R11P
D
ΔphoP Double Mutations
Absorbance
Time (min)
Cecropin A
Carbenicillin
Poly-B
PG-1
RR910LP
RR1011LP

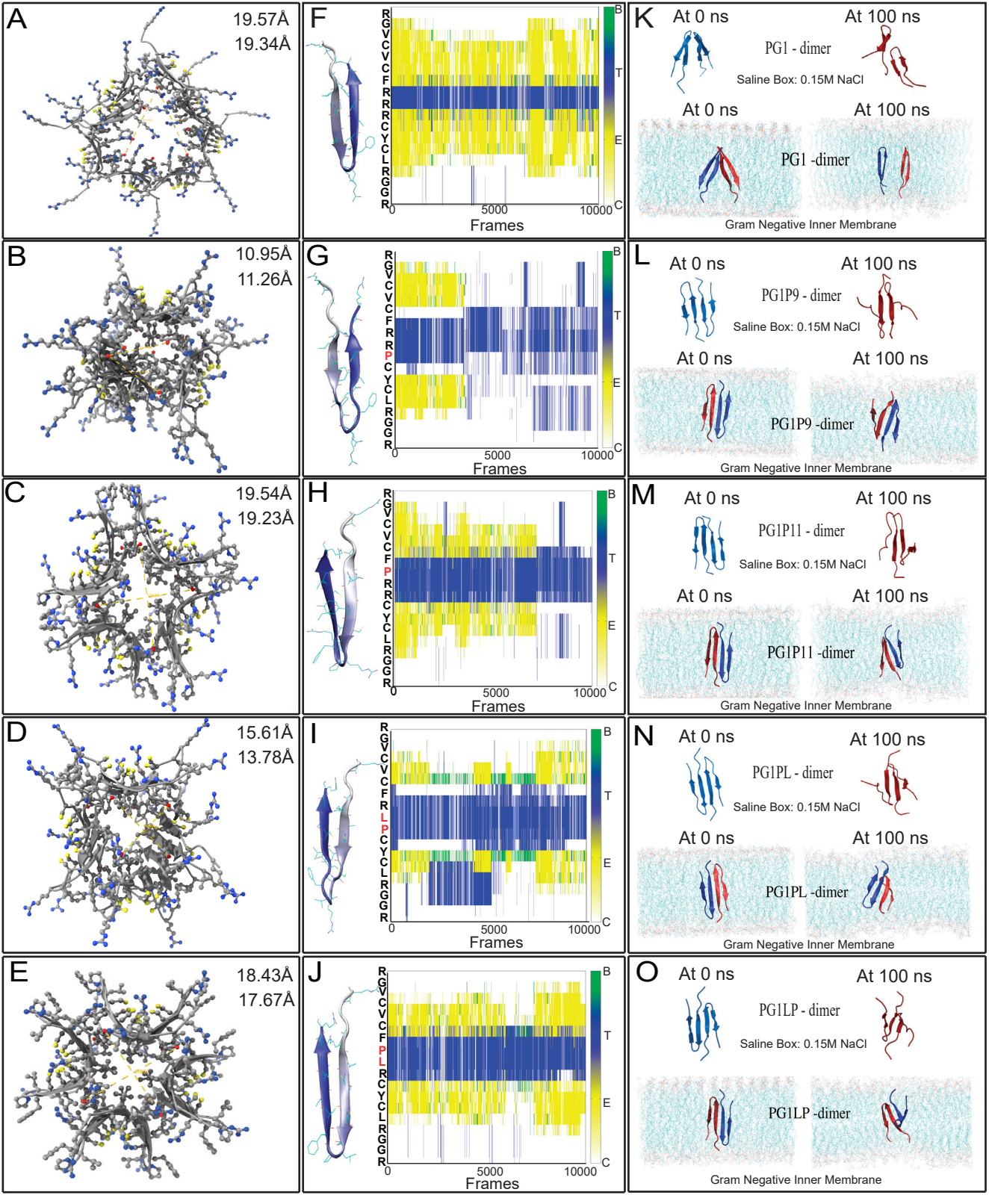
A
19.57Å
19.34Å
B
10.95Å
11.26Å
C
19.54Å
19.23Å
D
15.61Å
13.78Å
E
18.43Å
17.67Å
F
G
H
I
J
R G V C V C F R R R C Y C L R G G R
R G V C V C F R R P C Y C L R G G R
R G V C V C F P R R C Y C L R G G R
R G V C V C F R L P C Y C L R G G R
R G V C V C F P L R C Y C L R G G R
B
T
E
C
0
5000
10000
Frames
K
L
M
N
O
At 0 ns
At 100 ns
PG1 - dimer
PG1 -dimer
PG1P9 - dimer
PG1P9 -dimer
PG1P11 - dimer
PG1P11 -dimer
PG1PL - dimer
PG1PL -dimer
PG1LP - dimer
PG1LP -dimer
Saline Box: 0.15M NaCl
Gram Negative Inner Membrane